Journal of Building Engineering 71 (2023) 106421

Contents lists available at ScienceDirect

Journal of Building Engineering

journal homepage: www.elsevier.com/locate/jobe

Resilience and sustainability-informed probabilistic multi-criteria decision-making framework for design solutions selection

Jiajun Du [a,b], Wei Wang [a,b,*], Ting Lou [a,b], Hongyu Zhou [c]

[a] State Key Laboratory of Disaster Reduction in Civil Engineering, Tongji University, Shanghai, 200092, China
[b] Department of Structural Engineering, Tongji University, Shanghai, 200092, China
[c] Department of Civil and Environmental Engineering, University of Tennessee, Knoxville, TN, 37996, USA

ARTICLE INFO

Keywords:
Building holistic design
Seismic resilience
Sustainability
Life-cycle thinking
Multi-criteria decision-making
Monte Carlo simulation

ABSTRACT

In this paper, a novel probabilistic multi-criteria decision-making (MCDM) framework for sustainable and resilient building design solutions selection is developed to optimize alternatives or rehabilitation strategies in a life cycle context. The proposed framework holistically takes into account the buildings' resilience metrics, environmental sustainability, and energy consumption. The life cycle economic cost, global warming potential (GWP), primary energy use (PEU), and social impact are used to represent the buildings' resilience and sustainability. The second-generation Performance-based Earthquake Engineering procedure and FEMA P-58 method for time-based seismic performance analyses are used to evaluate earthquake-induced impact. The whole-building energy modeling (BEM) is adopted to assess energy use during the operational phase. In addition, life cycle analysis (LCA) and life cycle cost analysis (LCCA) are carried out to assess the life cycle performance of different design alternatives regarding environmental impacts and cost, respectively. Aiming to consider the various uncertainties in the decision-making process, a novel MCS-MCDM method is developed by combining the Monte Carlo simulation (MCS) with the traditional MCDM method. The proposed framework is applied to analyze hypothetical cases considering different geographic locations, structural systems, and building envelope systems, and recommendations are given according to the analysis results. The case study demonstrates the advantages of the proposed framework over traditional frameworks and its guidance for architectural design decisions.

1. Introduction

As reported by the World Green Building Council [1], the building sector accounted for 36% of the final energy consumption and 39% of the carbon dioxide (CO_2) emissions worldwide, becoming one of the leading causes of climate change and resource crisis. This has truly promoted the incorporation of sustainability considerations into the design process, such as the American Leadership in Energy and Environmental Design [2]. However, these sustainability assessments focus only on high-probability and low-consequence events (e.g., embodied carbon and operational energy use) in regular conditions, while the low-probability and high-consequence events (e.g., earthquakes) are largely overlooked [3]. The latter is generally related to buildings' hazard resilience performance [4]. The substantial recovery costs and long-term development stagnation caused by several significant earthquakes (e.g., 1994 Northridge, California and 2008 Wenchuan, China) [5,6] have proved that buildings' sustainability goals cannot be achieved without

* Corresponding author. State Key Laboratory of Disaster Reduction in Civil Engineering, Tongji University, Shanghai, 200092, China.
E-mail address: weiwang@tongji.edu.cn (W. Wang).

https://doi.org/10.1016/j.jobe.2023.106421
Received 30 December 2022; Received in revised form 27 February 2023; Accepted 28 March 2023
Available online 6 April 2023

considering hazard resilience. Thus, the main pillars of resilience and sustainability (i.e., economy, technical, organizational, ecology, and society) need to be comprehensively considered to achieve real sustainable development. An integrated design process can help with this, which incorporates various systems (e.g., environmental systems, energy systems, and human systems) throughout different phases of a building's life cycle (e.g., initial construction, operational, hazards experience, and maintenance, up to demolish) [7]. Many factors, such as modeling uncertainties, incomplete information, and different preferences of decision-makers, make this task challenging. Therefore, it is crucial to develop a life cycle thinking (LCT) based decision-making framework that can make the optimal and robust decision amongst alternatives when facing the challenge mentioned above.

To date, a number of studies have aimed to incorporate sustainability metrics into resilience assessment framework. Bocchini et al. [3] studied the relationship between resilience and sustainability, and then presented a unified approach to consider them for civil infrastructure. Chhabra et al. [8] proposed a rational probabilistic approach to quantify the life-cycle environmental performance of buildings due to seismic events. Dong and Frangopol [9] illustrated the seismic resilience and sustainability advantages of base-isolated steel structures over conventional structures in terms of economic loss, downtime, casualties, and carbon emission. Asadi et al. [10] evaluated the earthquake-induced economic, time, life, and environmental loss of steel diagrid structures, and demonstrated the benefits of sustainable design techniques through the use of recyclable materials. Anwar et al. [11] developed a performance-based decision-making framework for retrofit alternatives selection problems, which considers seismic resilience and sustainability. These excellent efforts have driven the implementation of sustainability metrics in resilience assessment. Since 2018, the environmental impact data has been added to the latest FEMA P-58 fragility database [12]. However, the above research mainly served for the design of structural systems rather than the whole building system. And most studies include embodied carbon emissions or energy use caused by seismic hazards as the most critical sustainability metric. Few of them fully considered the whole building life cycle, especially the operational phase.

A holistic assessment of the environmental impact of a building must cover a comprehensive consideration of its operational and embodied energy, and incorporate the consequences of hazard-induced damage [13,14]. Hasik et al. [15] developed a framework for the quantitative assessment of a range of sustainability and resilience performance aspects by bringing together multiple developed methods, such as LCC, LCA, energy modeling, and seismic loss estimation. Mosalam et al. [7] used performance-based engineering method to assess the building's structural safety and energy efficiency in an integrated manner. Shen et al. [16] carried out a life cycle cost analysis for building structures and building envelope systems, which comprehensively considered the building's energy efficiency and seismic performance. Asadi et al. [17] integrated the building's sustainability, energy, and resilience performance into a holistic risk-informed assessment for reinforced concrete buildings. However, few holistic assessments discussed the uncertainties of building energy simulation, which may influence the life cycle assessment [18].

To measure the building life cycle performance, a common strategy is to translate all impacts into a common utility, measured in monetary costs [19,20]. But in actual decision-making, economic loss is usually not the only criterion of concern. Meanwhile, criteria may be contradictory in some cases. For example, resilient design targets safety and durability, and is therefore accompanied by redundancy, which is often conflicting with sustainability guidelines [21]. Similarly, high-performance envelope materials and assemblies will bring high energy savings, but they may cause higher losses and casualties in earthquakes due to their excessive vulnerability [16].

Many researchers have emphasized the necessity of adopting a multi-criteria decision-making (MCDM) approach due to the variety of criteria involved in the design process [7,10,17]. Analytical Hierarchy Process (AHP) first developed by Saaty [22] is a widely used MCDM method and has been used in resilience and sustainability decision-making problems [17]. But the traditional AHP method has oftentimes been critiqued for using exact values to represent the decision-makers' opinions. Moreover, since the average value is used, it cannot reflect the different preferences among several decision-makers [23,24]. Combining Monte Carlo Simulation (MCS) with the AHP method is considered an effective way to address these issues and has played an effective role in selecting the optimum mining method [25]. The subjective weights obtained from the AHP method can be combined with the objective weights from the Entropy Weight Method (EWM) derived from Shannon's information theory [26] to form a combined weight to avoid excessive subjectivity or objectivity of the weights [27–29]. Technique for Order Preference by Similarity to Ideal Solution (TOPSIS) [30] is another broadly used MCDM method that has been used in existing building holistic design studies [10,11]. However, due to methodological limitations, the expected value is used as a basis for ranking rather than the resulting statistical distribution obtained by assessment. This deficiency weakens the robustness of the decision. According to the best of authors' knowledge, a fully integrated building life cycle resilience and sustainability decision-making framework considering various uncertainties (especially the uncertainties of building energy simulation) is still not well developed.

This paper proposed a novel resilience and sustainability-informed probabilistic MCDM framework for building design solutions selection in the life cycle context. Economic cost, global warming potential (GWP), primary energy use (PEU), and social impact are selected as the primary criteria. The first three criteria are measured from a life cycle perspective, and each is further subdivided into three components, i.e., hazards-induced component, operational component, and another component including initial construction, maintenance, and demolish. As for the social impact, casualties and downtime caused by earthquakes are selected as two subcriteria. The hazards-induced component and social impact can be obtained through the second-generation Performance-Based Earthquake Engineering (PBEE-2) [31] and FEMA P-58 [12] method. Operational energy use is obtained using whole-Building Energy Modeling (BEM), and the uncertainties of glazing properties, occupancy, and lighting intensity are considered. Other components of the first three criteria can be obtained by conducting traditional life cycle analysis (LCA) and life cycle cost analysis (LCCA), which evaluate the life cycle performance of different design alternatives, in terms of environmental impacts and cost, respectively. To overcome the shortcomings of existing MCDM methods, a novel approach is proposed in this paper, which combines the Monte Carlo simulation with the traditional MCDM method. The detailed procedure of the proposed framework is given in Section 2. And then, the proposed

framework is implemented to analyze hypothetical cases considering different geographic locations, structural systems, and building envelope systems, which are discussed in Section 3.

2. Proposed framework

Fig. 1 illustrates the proposed three-stage MCDM framework for the selection of building design solutions. The framework is intended to provide a comprehensive view of the assessment of building structures and envelope systems considering seismic resilience and sustainability in the life cycle context. In the first stage, decision-makers need to select the criteria according to their preferences and design target, which are described further in Section 2.1. In the second stage, LCA, LCCA, PBEE-2, and BEM will be carried out to assess the buildings' performance under the selected criteria, which are elaborated in Section 2.2. Once the assessment is completed, an MCS-MCDM process will be carried out in the third stage to help designers choose the optimum from the alternatives, which are introduced in Section 2.3.

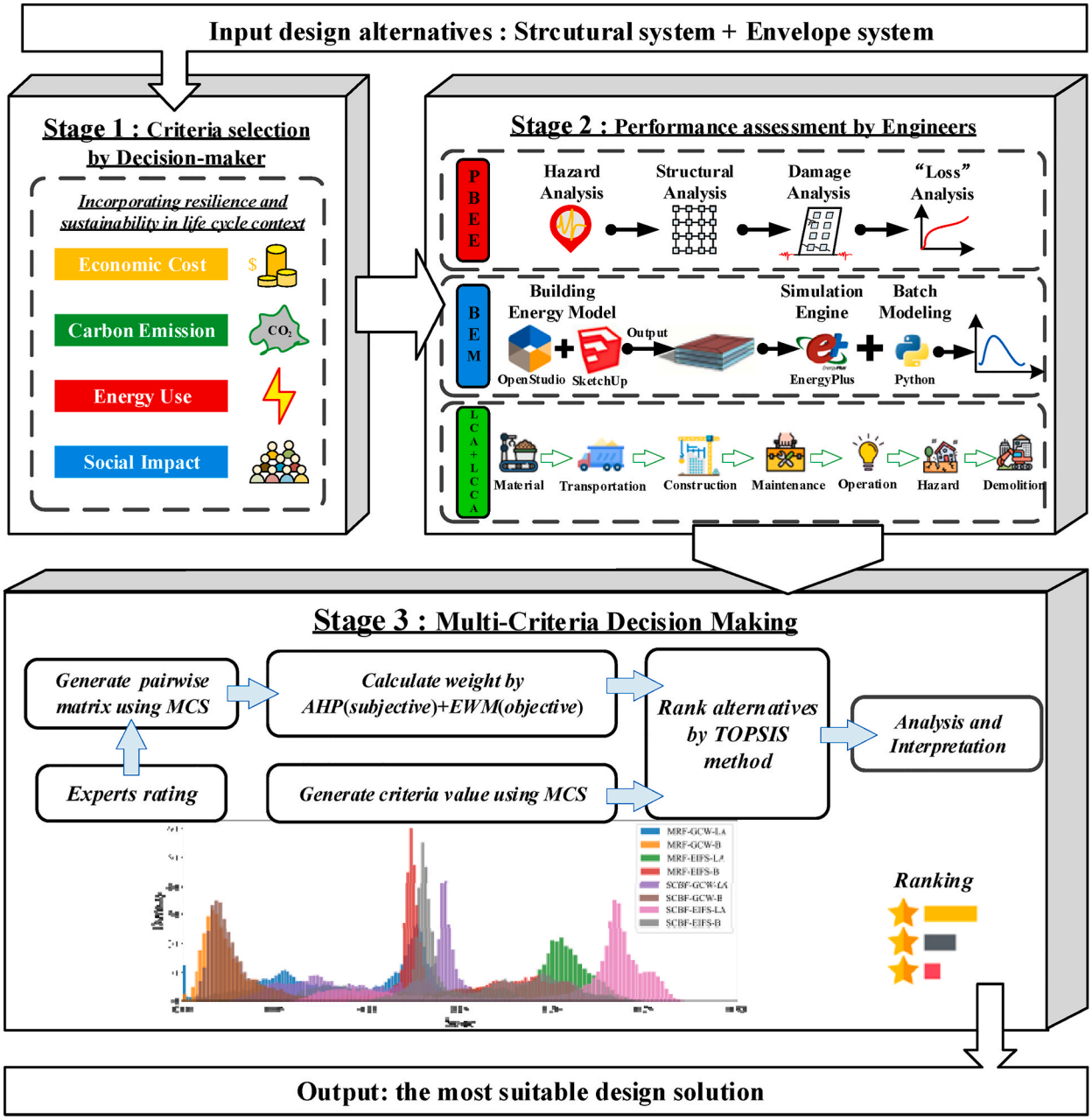

Fig. 1. Proposed MCDM framework in this paper.

2.1. Criteria selection

The principle of selecting criteria in this paper is to comprehensively consider the resilience and sustainability of a building in its life cycle context. Both resilience and sustainability use social and economic categories as a basis for the assessment. Specifically, in existing studies on the seismic resilience of individual buildings, the economic loss, human casualties, and the time required to recover to its original function after a building suffers an earthquake have been closely concerned. In contrast, for green sustainable buildings, more attention has been paid to the environmental impacts generated by the buildings, such as carbon emissions and energy consumption.

Considering the above, life cycle economic cost, life cycle GWP, life cycle PEU, and social impact are selected to reflect the main pillars of sustainability and resilience. The definition of a building's life cycle is described in Section 2.2.1. Quantifying the social impact of a building is a complex problem, and its research is still in the development stage. Therefore, this study only considers the social impact caused by the earthquake as an illustration, i.e., downtime and casualties, which is commonly used in existing research [10–12,20,32,33]. Downtime reflects the time required for a building to fully recover after an earthquake. The seismic resilience is reflected by the earthquake-induced component of each criterion, i.e., earthquake-induced economic cost, GWP, PEU, casualties, and downtime. Meanwhile, the selected criteria fit into the three pillars of sustainability, i.e., economy, ecology, society. Note that to measure the environmental aspect of sustainability, a suite of criteria can be used from current standards for LCA. Amongst these criteria, GWP (measured in CO_2 equivalents) and PEU are recommended as the environmental indicators for this paper according to FEMA P-58 [12].

2.2. Performance assessment

2.2.1. LCA and LCCA

LCA is a methodology for assessing various environmental impacts associated with all the life cycle phases of a building [34]. However, LCA does not account for economic aspects, and such analysis should therefore be considered together with the LCCA [35]. As shown in Fig. 2, there are seven phases in a building's life cycle, including building material production, transportation, construction, operation, maintenance, and demolition. Hence, the life cycle cost can be calculated as:

$$LC_{\mathrm{Cost}}(T_{\mathrm{sl}}) = C_{\mathrm{IC}} + C_{\mathrm{M}}(T_{\mathrm{sl}}) + C_{\mathrm{O}}(T_{\mathrm{sl}}) + C_{\mathrm{H}}(T_{\mathrm{sl}}) + C_{\mathrm{D}} \tag{1}$$

where C_{IC} is the initial construction cost (including building materials, transportation and construction); $C_{\mathrm{M}}(T_{\mathrm{sl}})$ is the maintenance cost; $C_{\mathrm{O}}(T_{\mathrm{sl}})$ is the operational energy cost; $C_{\mathrm{H}}(T_{\mathrm{sl}})$ is the hazards (e.g., earthquakes) induced cost of the building; C_{D} is the demolish cost; T_{sl} is the building's expected service life, which is usually 50 years for ordinary commercial buildings.

The life cycle cost, $C_{\mathrm{M}}(T_{\mathrm{sl}})$, $C_{\mathrm{O}}(T_{\mathrm{sl}})$, can be estimated by discounting the annual cost to present by Eq. (2).

$$C(T_{\mathrm{sl}}) = \sum_{j=1}^{T_{\mathrm{sl}}} \left(\frac{1}{1+\alpha}\right)^{j} C^{annual} \tag{2}$$

where C represents C_{M} or C_{O}; α is the discount rate, which is 0.3 in this paper.

Note that unlike previous literature that translates earthquake losses into annual expected earthquake losses, this paper samples the loss probability curves obtained from PBEE-2 procedure and uses random numbers to acquire the loss cost, C_{H}^{sample}, and the time of occurrence (which year), y. The detailed sampling process will be further described in Section 2.3. And then the net present value of hazards-induced cost $C_{\mathrm{H}}(T_{\mathrm{sl}})$ can be calculated as:

$$C_{\mathrm{H}}(T_{\mathrm{sl}}) = \left(\frac{1}{1+\alpha}\right)^{y} C_{\mathrm{H}}^{sample} \tag{3}$$

Similar to the economic cost, the life cycle GWP and PEU can be calculated by equation (3) and equation (4), respectively.

$$LC_{\mathrm{GWP}}(T_{sl}) = GWP_{\mathrm{IC}} + GWP_{\mathrm{M}}(T_{\mathrm{sl}}) + GWP_{\mathrm{O}}(T_{\mathrm{sl}}) + GWP_{\mathrm{H}}(T_{\mathrm{sl}}) + GWP_{\mathrm{D}} \tag{4}$$

$$LC_{\mathrm{PEU}}(T_{\mathrm{sl}}) = PEU_{\mathrm{IC}} + PEU_{\mathrm{M}}(T_{\mathrm{sl}}) + PEU_{\mathrm{O}}(T_{\mathrm{sl}}) + PEU_{\mathrm{H}}(T_{\mathrm{sl}}) + PEU_{\mathrm{D}} \tag{5}$$

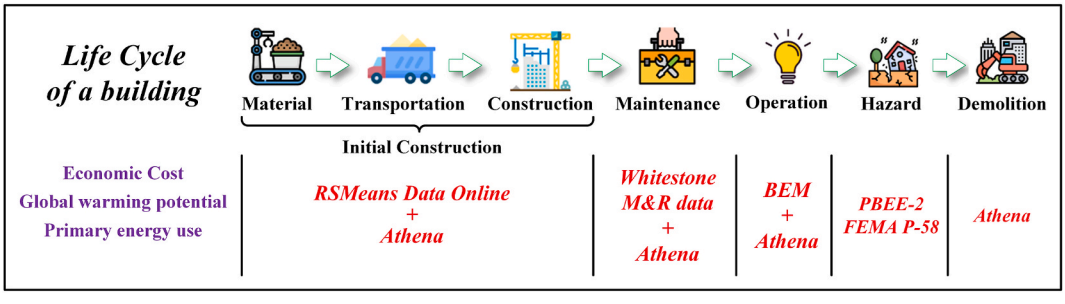

Fig. 2. Schematic diagram of a building's whole life.

The initial construction cost C_{IC} and the maintenance cost $C_M(T_{sl})$ are estimated using the RSMeans [36] and Whitestone M&R data [37] respectively. The annual operational cost $C_O(T_{sl})$ can be calculated by the local energy prices and the operational energy use ($PEU_O(T_{sl})$) obtained by the BEM. The items related to GWP and PEU (except for $GWP_H(T_{sl})$, $PEU_H(T_{sl})$) can be estimated with the Athena Impact Estimator [38], which is specifically developed for the LCA of complete buildings. The earthquake-induced items (e.g., $C_H(T_{sl})$, $GWP_H(T_{sl})$, $PEU_H(T_{sl})$, casualties, and downtime) can be calculated through PBEE-2 framework and FEMA P-58 method.

2.2.2. PBEE-2 framework

The PBEE-2 framework for assessing a building's probable seismic performance was developed by the Pacific Earthquake Engineering Research center [39]. Detailed practical methodology and guidance can be found in the FEMA P-58 documentation [12]. In this framework, the probability of exceeding a specific "loss" value for a given intensity measure (IM) is expressed as:

$$P(loss|IM) = \int_{DM}\int_{EDP} P(loss|DM)|dP(DM|EDP)||dP(EDP|IM)| \tag{6}$$

where $P(EDP|IM)$ is the probability of exceeding an engineering demand parameter (EDP) for a given IM. $P(DM|EDP)$ is the probability of exceeding a damage measure (DM) for a given EDP. $P(loss|DM)$ is the probability of exceeding a "loss" for a given DM. The "loss" herein represents the cost, GWP, PEU, downtime, and casualties induced by earthquakes; IM is the earthquake intensity measure represented by the 5% damped spectral acceleration at the fundamental period of the studied structure, denoted as $S_a(T_1)$; DM refers to discrete damage states of building components, which are given based on expert judgment on experiments, and each damage state is allocated a consequence (i.e., repair cost, GWP, PEU, casualties and repair time); EDP is the most relevant structural response parameter to the damage states.

The PBEE-2 procedure utilizes four steps to quantify the earthquake-induced impacts for a given building. The details of the four steps (as illustrated in Fig. 3) are as follows:

1) *Hazard analysis.* A suite of site-specific hazard curves can be obtained from specific hazard analysis applications or governmental websites, e.g., OpenSHA or the U.S. Geological Survey (USGS) website [40], with regard to the building's location and site condition. These curves give the relationship between the annual probability of exceedance of seismic hazard and the seismic IM, which will be used for time-based assessment.
2) *Structural analysis.* The main task in this step is to establish numerical structural models for the given building and determine its EDP (e.g., the peak inter-story drift ratio (PIDR), and the peak floor acceleration (PFA)). Collapse fragility and the distributions of EDPs are obtained via incremental dynamic analysis (IDA) [41]. The quantities of IMs and ground motions used in IDA were denoted as N_{IM} and N_{GM}, and a total of $N_{IM} \times N_{GM}$ nonlinear dynamic analyses are performed. Each set of EDPs can be derived from each time history analysis. A sufficient number of nonlinear analyses is required to fully consider the uncertainties of structural model and ground motions, which is usually impractical due to high computational and time costs. An algorithm first proposed by Yang et al. [42] and improved by FEMA P-58 is used to generate a large number of realizations according to

$$EDP_{gen} = \exp\left(L_{\mathrm{cov}(\ln\ edp)} D_{\mathrm{cov}(\ln\ edp)} U + M_{\ln\ edp}\right) \tag{7}$$

where *edp* is matrix of EDPs obtained from IDA (the number of rows = N_{GM}, the number of columns = the number of EDP variables (denoted as *n*)); cov(ln*edp*) is an $n \times n$ matrix equal to the covariance matrix of the natural logarithmic matrix of *edp*; $L_{\mathrm{cov}(\ln edp)}$ is an $n \times n$ matrix equal to the eigenvector matrix of cov(ln*edp*); $D_{\mathrm{cov}(\ln edp)}$ is an $n \times n$ matrix equal to the square-root of eigenvalues of

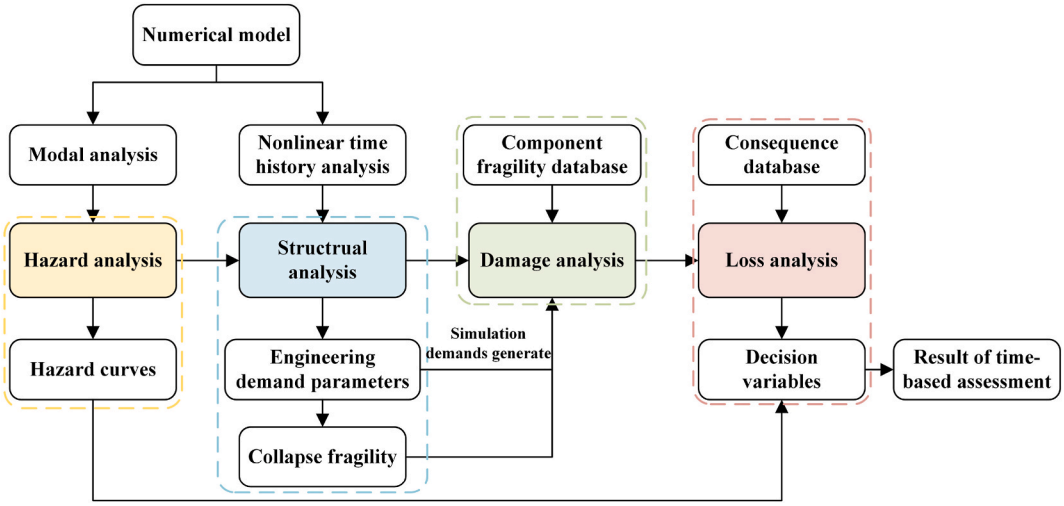

Fig. 3. Illustration of the PBEE-2 procedures.

covariance matrix cov(ln*edp*); *U* is a column vector of zero mean uncorrelated Gaussian random variables, which is an $N_R \times 1$ matrix (N_R = the number of EDPs set expected to generate); $M_{\ln edp}$ is a column vector containing mean values of ln*edp*; EDP_{gen} is the result simulated demands, which is an $N_R \times$ n matrix. Each row in EDP_{gen} represents one simulated EDP set, which is termed a 'realization'.

3) *Damage analysis.* In this step, a building may experience three different states, i.e., collapse, irreparable, and repairable. First, it is determined whether or not collapse has happened. The collapse possibility for a given IM, $P(C|IM)$, is determined using the collapse fragility function acquired through the IDA. Then, $P(C|IM) \times N_R$ is judged to have collapsed. After collapse determination, the maximum residual inter-story drift ratio (RIDR) is taken as the criterion to judge reparability for the rest $(1\text{-}P(C|IM)) \times N_R$ realizations. According to FEMA P-58 [12], the maximum RIDR above which the structure could be irreparable is assumed to follow a lognormal distribution with median and dispersion equal to 1% and 0.3, respectively. If the building is neither collapsed nor irreparable, each component's damage state is determined using the set of generated demands. Each building component has an associated series of damage states and fragility functions. The fragility functions describe the probability that components will be damaged to a given level under a specific EDP.
4) *Loss analysis.* If a realization is judged to occur collapse or excessive RIDR induced irreparable, its "loss" should equal the replacement consequences. For the remaining realizations, neither collapse nor irreparable, random sampling is carried out according to the statistical distribution of consequences corresponding to the damage state of each component determined in the damage analysis. The distributions of the consequences under every given IM can be obtained by aggregating the results of N_R realizations. The above procedure can give the possible seismic performance considering all interested IMs of the earthquake that the building may experience within its service life.

The annual exceedance probability (AEP) of a certain "loss" (denoted as λ) can be determined by weighting the performance outcome from each IM by the AEP of such intensity of shaking (denoted as $\lambda(\mathrm{IM})$), as expressed as:

$$\lambda = \int_0^{\infty} P(loss|IM) \left| \frac{d\lambda(IM)}{dIM} \right| dIM \tag{8}$$

Assuming that the occurrence of an earthquake within a given time is a Poisson distribution, the AEP of "loss" within a specific time period *T*, $P(loss|T)$, can be calculated by Eq. (9).

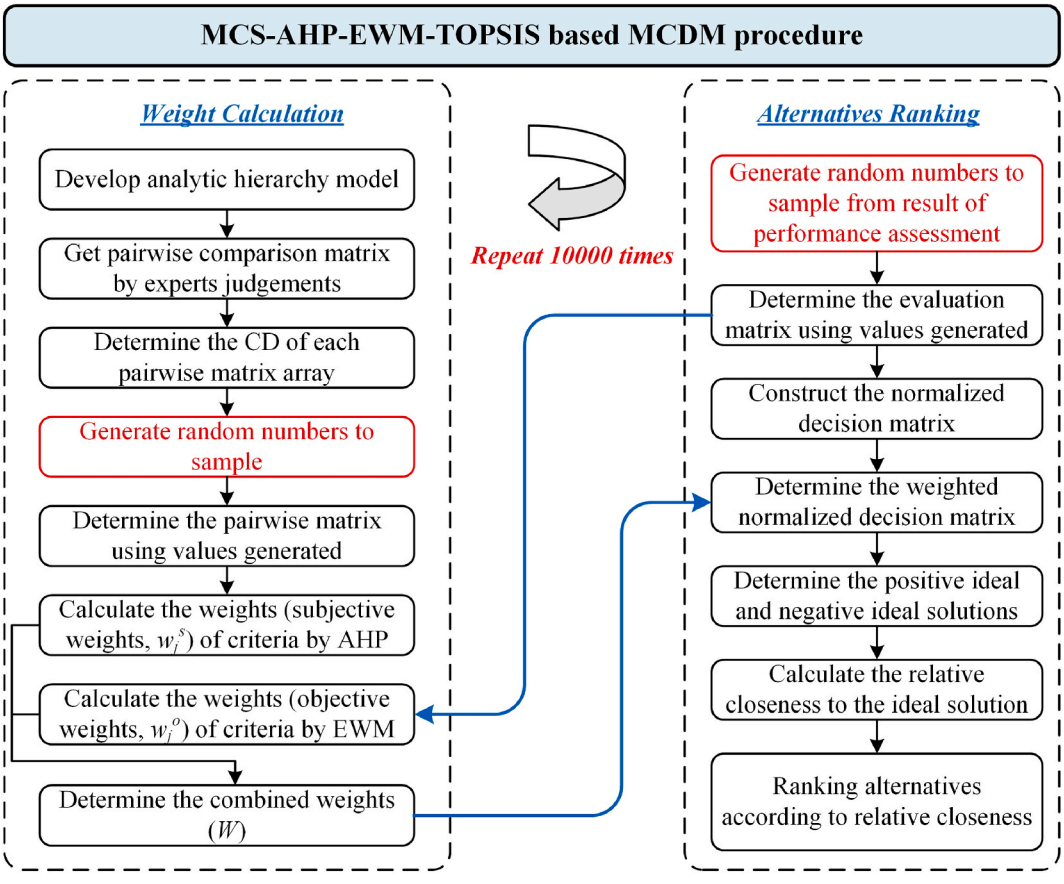

Fig. 4. Flowchart for proposed MCS - MCDM procedure.

$$P(loss|T) = 1 - e^{-\lambda T} \tag{9}$$

2.2.3. Building energy modeling

The impact of the operational phase of a building is critical in the whole life cycle. For conventional buildings, operational energy use constitutes 80%–90% of life cycle energy use [43]. The energy demand estimation process can be carried out using whole-building energy simulation software, such as EnergyPlus [44]. However, deterministic simulation results may not represent the actual energy performance, which directly affects the subsequent evaluation of design alternatives [18]. Hence, Monte-Carlo simulation is combined with building energy simulation in this proposed framework, as shown in the BEM part of Stage 2 in Fig. 1. The 3D design software SketchUp [45] and whole building energy modeling software OpenStudio [46] are combined to model the geometry and detailed property setting of the building's energy model. Then, parametric models are established through an application programming interface (API) for EnergyPlus, named eppy [47], based on the IDF file exported from OpenStudio and calculate the building energy use. In this step, three input parameters, i.e., glazing properties, occupancy, and lighting intensity, which may significantly affect the output results are considered variables with associated uncertainties. To improve the convergence efficiency and reduce the computational cost, the Monte Carlo Latin Hypercube Sampling (LHS) [48] is carried out to generate samples. Note that, in addition to the uncertainties of some properties of the building itself and its internal as considered in this paper, there are many other factors that affect the building energy simulation, such as the building orientation [49], the input weather file [50], the building surroundings [51], etc.

2.3. MCS - MCDM procedure

The proposed MCS-MCDM procedure for addressing the challenges in building design solutions selection consists of two steps, i.e., weight calculation and alternatives ranking. Experts qualitatively determine the weight of criteria, and then the criteria assigned with weights are used to evaluate alternatives. Specifically, first, the MCS – AHP – EWM method is used to generate the weight of each criterion considering the uncertainty of experts' opinions. Second, the MCS–TOPSIS method is used to score and rank the alternatives considering the uncertainty of performance assessment. The detailed process is illustrated in Fig. 4.

2.3.1. Weight calculation: MCS – AHP - EWM method

To date, a number of methods have been proposed to yield weights in MCDM issues, including objective and subjective weight methods. Objective weight methods, such as the variation coefficient method and entropy weight method (EWM), determine weights based on the information provided by evaluation matrix itself but overlook the decision-makers' preferences. Subjective weight methods, such as the Delphi method and AHP method, determine weights based on experts' experience and judgment but may be susceptible to subjective arbitrariness. Hence, this paper uses a combination weight method, which integrates the AHP and EWM, to obtain the optimized weights. The method used is considered to effectively utilize both methods according to existing studies [27–29, 52,53].

EWM is a commonly used objective weighting method that measures value dispersion in decision-making. The greater the degree of dispersion, the more information can be derived, and a higher weight should be given to the index [54]. AHP is a combination of qualitative and quantitative decision-making analysis methods. The core idea of the AHP is to decompose a complex problem into several levels and factors, and then assign weights and rankings to each factor. Although AHP has been widely used, they are still criticized for using a deterministic value to express the decision makers' judgment in alternatives comparison process. Agreement or disagreement between decision-makers regarding the element of pairwise matrix is also not investigable [25]. Combining Monte Carlo simulation with AHP is considered an effective means of overcoming these drawbacks and has been applied in other fields [25,55]. The

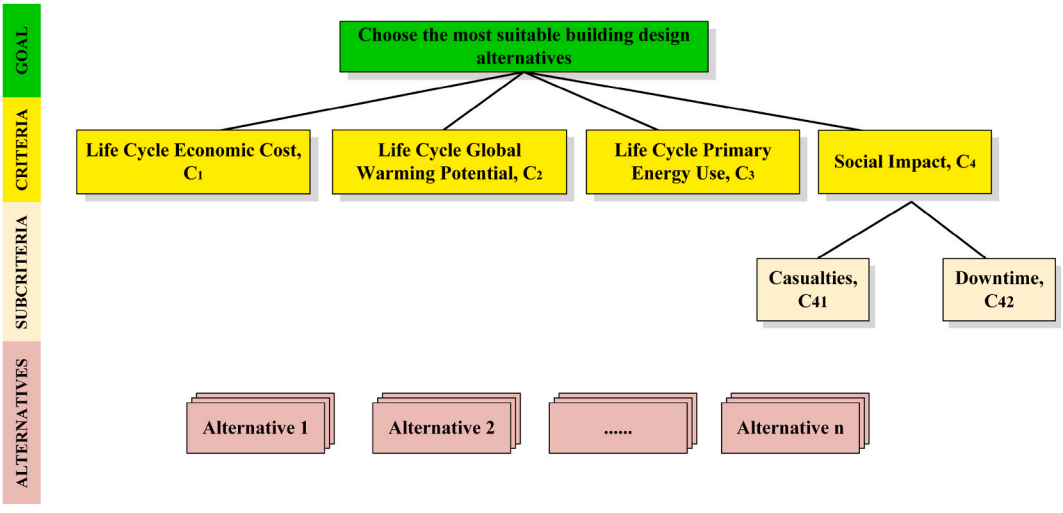

Fig. 5. Analytic hierarchy model considered for decision making.

main steps of using the MCS-AHP-EWM to get criteria weights are as follows:

1) Identify decision-making problem's objectives, criteria, and alternatives to construct the analytic hierarchy model, as shown in Fig. 5.
2) Compare the importance degree between every two criteria by using a pairwise comparison with Saaty's scale as shown in Table 1. Assume the number of criteria is n, $\frac{n(n-1)}{2}$ judgments are made to create a set of matrices. Combine the above $\frac{n(n-1)}{2}$ matrices into a global matrix.
3) Determine the pairwise matrixes of each decision maker by using step 1–2. These matrixes form a 3D matrix, where the third dimension is the number of decision-makers.
4) Determine the cumulative distribution (CD) of each pairwise matrix array.
5) Generate a sample between 0 and 1, and allocate a value for each random number by using the CD.
6) Determine the pairwise matrix using values generated in step 5.
7) Calculate the maximum eigenvalue of the matrix to get the ranking and weights of different criteria. The subjective weights obtained here are denoted as w_j^s.
8) Implement the standardization of the evaluation matrix. The evaluation matrix in the second step of MCS-TOPSIS method mentioned later in Section 2.3.2 is used here to calculate the objective weights through EWM. The standardized value of the i^{th} alternatives in the j^{th} criteria is denoted as p_{ij}, and can be calculated as:

$$p_{ij} = \frac{x_{ij}}{\sum_{i=1}^{n} x_{ij}} \tag{10}$$

9) Define the entropy value E_j of the j^{th} criterion as:

$$E_j = \frac{\sum_{i=1}^{n} p_{ij} \cdot \ln p_{ij}}{\ln n} \quad \text{if } p_{ij} = 0, \text{then } p_{ij} \cdot \ln p_{ij} = 0 \tag{11}$$

10) Calculate the objective weight by EWM as:

$$w_j^o = \frac{1 - E_j}{\sum_{j=1}^{m} (1 - E_j)} \tag{12}$$

11) Determine the final composite criteria weight (W) from both objective and subjective weights as [27]:

$$W = \frac{w_j^o w_j^s}{\sum_{j=1}^{m} w_j^o w_j^s}, \forall j \tag{13}$$

2.3.2. Alternatives ranking: MCS-TOPSIS method

After getting the combination weights, the next step is to adopt the MCS-TOPSIS method as the ranking method for the alternatives. TOPSIS method ranks the alternatives by calculating the relative closeness of each solution to the ideal solution, and thus selects the optimal solution. But the traditional TOPSIS method is not applicable in cases when the criteria attribute values are probabilistically statistically distributed. For such cases, the mean value of the statistical distribution is usually used as the criteria attribute value, but this behavior weakens the effort we have made in the performance assessment stage. Thus, once again the MCS is used to transfer uncertainties into the final decision. The MCS-TOPSIS method is carried out as follows:

1) Generate random numbers to sample from the results of the performance assessment mentioned in Section 2.2.
2) Create an evaluation matrix consisting of m criteria and n alternatives using values generated in step 1, with the intersection of each alternative i and criteria j given as x_{ij}, then a matrix $(x_{ij})_{n\times m}$ is obtained.
3) Construct a normalized decision matrix.

$$r_{ij} = x_{ij} \Big/ \sqrt{\sum_{i=1}^{n} x_{ij}^2} \tag{14}$$

Table 1
Pairwise comparisons with Saaty's scale.

Importance	Definition
1	Equal importance
3	Moderate/weak importance of one over another
5	Essential or strong importance
7	Demonstrated importance
9	Absolute importance
2, 4, 6, 8	Intermediate values between the two adjacent judgments

4) Construct the weighted normalized decision matrix using the criteria weight (W) obtained.

$$z_{ij} = Wr_{ij} \tag{15}$$

5) Determine the positive ideal and negative ideal solutions.

The positive ideal solution:

$$Z^+ = \left(Z_1^+, Z_2^+, ..., Z_m^+\right), Z_j^+ = \left\{\max\left(z_{ij}\right)\right\} \tag{16}$$

The negative ideal solution:

$$Z^- = \left(Z_1^-, Z_2^-, ..., Z_m^-\right), Z_j^- = \left\{\min\left(z_{ij}\right)\right\} \tag{17}$$

6) Calculate the distance between each alternative and the positive (negative) ideal solutions D_i^+ (D_i^-).

$$D_i^+ = \sqrt{\sum_{j=1}^{m}\left(Z_j^+ - z_{ij}\right)^2} \tag{18}$$

$$D_i^- = \sqrt{\sum_{j=1}^{m}\left(Z_j^- - z_{ij}\right)^2} \tag{19}$$

7) Calculate the relative closeness to the ideal solution S_i. And select the alternative with S_i closest to 1.

$$S_i = \frac{D_i^-}{D_i^+ + D_i^-} \tag{20}$$

The MCDM process described above is repeated 10,000 times, with each decision-making process accompanied by different weights and performance inputs. The further detailed demonstration can be found in Section 3.5. The proposed MCS – MCDM procedure not only improves traditional decision-making methods, but also provides better adaptability to the challenges faced in the building design solutions selection process. The use of MCS allows various types of uncertainty in selection process to be transferred to the final decision result.

3. Case studies

3.1. Archetype configuration

To demonstrate the proposed framework, this section studied eight 3-story steel frame office building alternatives, which include two structural systems, two envelope systems, and two locations. Seismic levels and climatic conditions are most closely related to the

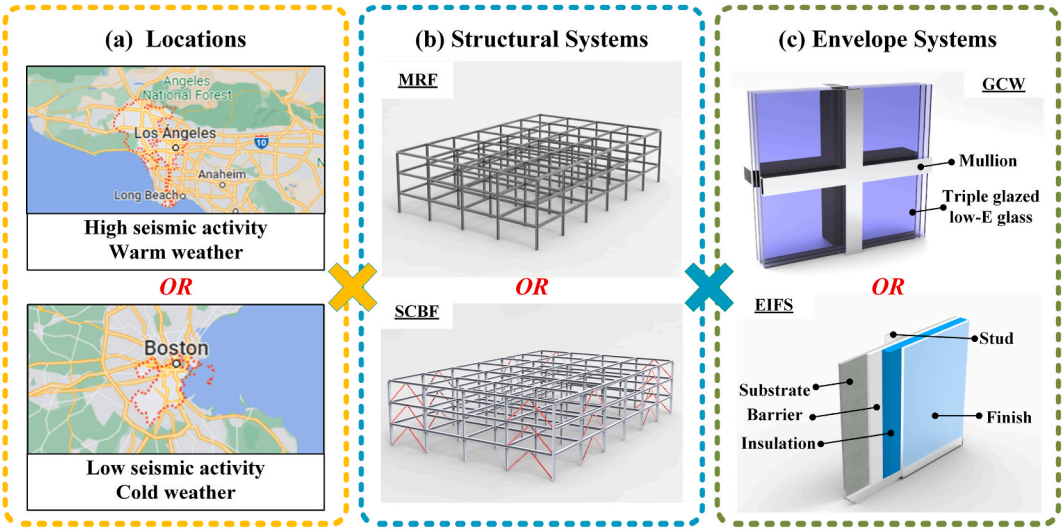

Fig. 6. Eight building alternatives considered in case studies.

structural systems and envelope systems, respectively. To better illustrate the variability of these two factors, two locations with different characteristics were selected, i.e., Los Angeles (LA) and Boston (B), as shown in Fig. 6 (a). The LA has a warm climate and high-level seismic activity. In contrast, Boston has a cold climate and low-level seismic activity. Note that only differences in climatic conditions and seismic levels due to locations are considered. The differences caused by different transportation assumptions or local electricity grids, or some others not related to climatic conditions or seismic activity are out of the scope of this study and are not considered.

The 3-story building is 36.58 m by 54.87 m in plan, and 11.89 m in elevation. Two widely used benchmark steel structures were considered, namely the moment-resisting frame (MRF) and special concentrically braced frame (SCBF), as illustrated in Fig. 6 (b). The MRF adopted from FEMA 355C [56] was designed by Brandow & Johnston Associates for the SAC Phase II Steel Project, which represents the typical low-rise office buildings designed for the Los Angeles, California region. The SCBF was designed following the same criteria so that it is capable of comparing structural performance with that of the MRF [57]. Note that for comparison purposes, alternatives in Boston used the same structural system parameters as in LA rather than redesigning a new structure. Both steel buildings have four bays in the N–S direction and six bays in the E-W direction. Each building's lateral load resisting system is comprised of steel perimeter MRFs or SCBFs with simple framing between the two furthest south E-W frames. The interior bays of the structure contain simple framing with composite floors. In addition, the component dimensions and related material properties can be found in Section 3.3.1 and more detailed design information can be found in Refs. [56–59]. SCBF represents a more efficient lateral force resistance system. Despite its increased diagonal bracing, it reduces the cross-section area of the beams and columns and uses less steel overall than MRF.

As for the envelope systems, the exterior insulation and finishing system (EIFS) and the glass curtain wall (GCW) are considered, as illustrated in Fig. 6 (c). The GCW needs more labor cost than the EIFS since it uses the mid-rise stick system, which involves the installation of mullions and spandrel panels [16]. In this section, triple-glazed low-E (TriLE) glass is selected as the glazing material for both GCW and EIFS's windows, and vacuum insulated panel (VIP) is selected as the insulation material for EIFS's insulation layer. For EIFS cladding, the window-to-wall ratio of EIFS cladding is set as 37.5%. Detailed information about the envelope systems is referred to Ref. [16] to meet ASHRAE 90.1 [60].

Tables 2 and 3 list the thermal properties of TriLE glazing material and EIFS's exterior wall, which be used for BEM.

3.2. LCCA and LCA for alternatives

Fig. 7 shows the life cycle stages and building systems included in this illustrative example. At the building scale, structural, enclosure, and some interior components are taken into account for both LCA and LCCA. Specifically, the "end of life" stage of a building's life cycle, such as demolition, is only included in LCA due to the lack of available data on demolition costs. On the other hand, the mechanical, electrical, and plumbing (MEP) systems of a building are only considered in LCCA because modeling them accurately in LCA can be challenging. In this study, LCA and LCCA are regarded as two independent methods that do not strictly require aligned scope and assumptions. Figuratively speaking, the two methods are treated as two experts in their respective fields, providing reasonable assessments based on their expertise respectively. In MCDM, different criteria, such as cost, carbon emission, and casualties, can be considered together, even if they have different units, meanings or are measured by different methods. Reasonable results can be achieved as long as the assumption for assessing individual criterion of building solutions is the same, without requiring the same assumptions for all criteria. Therefore, it is reasonable to consider the two methods as independent without comparing the LCCA and LCA results. To the authors' best knowledge, a comprehensive database including both cost and environmental impact for building's life cycle analysis does not yet exist, and the intersection between LCCA and LCA is still in the developmental stage. This study aims to show that both methods can work individually without the constraints of other methods' limitations. It is worth noting that the implications of this initiative need to be studied further in the future.

Building components considered and corresponding data are shown in Appendix Table A1, A2. RSMeans Data Online [36] is used to estimate the initial construction cost, which can consider materials, labor, and equipment costs of different regions in America. The initial construction cost includes the foundation cost, shell cost (i.e., floor and roof), beam-column frame cost, interiors cost, services cost, contractor fees and architectural fees. For the same configuration, the cost of Boston is generally higher than that of Los Angeles because of its higher labor cost. The maintenance cost is estimated by the Whitestone M&R data [37]. The service life of glazing materials is considered 30 years, i.e., the windows in EIFS and glass curtain will be replaced every 30 years [37]. Except for the periodic replacement of glazing material, the GCW requires a regular minor repair every 5 years, while the operable windows of EIFS are every 15 years [16]. For EIFS panels, annual inspection and minor repair expenses of 0.5 $/m^2 are anticipated, with regular maintenance every five years at a cost of 2 $/m^2 according to Ref. [16]. The maintenance costs of other components (e.g., interior finishes, plumbing, electrical facilities) are also considered according to the office building prototype in the Whitestone M&R data [37]. In addition, for Boston, the maintenance cost is 1.07 fold that of LA according to the local maintenance cost index provided in the Whitestone M&R data [37].

The GWP and PEU are calculated using the Athena Impact Estimator [38], which is the only free tool in North America designed to

Table 2
Solar thermal properties of TriLE glazing material.

Glazing Type	SHGC	Direct solar transmission	Visible Light transmission	U-value (W/m^{2}K)
TriLE	0.22	0.13	0.27	1.2

*SHGC = Solar heat gain coefficient.

Table 3
Thermal properties of exterior walls of EIFS.

EIFS-VIP	Thickness (mm)	Conductivity (W/mK)	Density (kg/m^3)	Specific Heat (J/kgK)
Stucco	25	0.72	1856	840
VIP	51	0.008	175	800
Plaster Board	12	0.58	800	1090

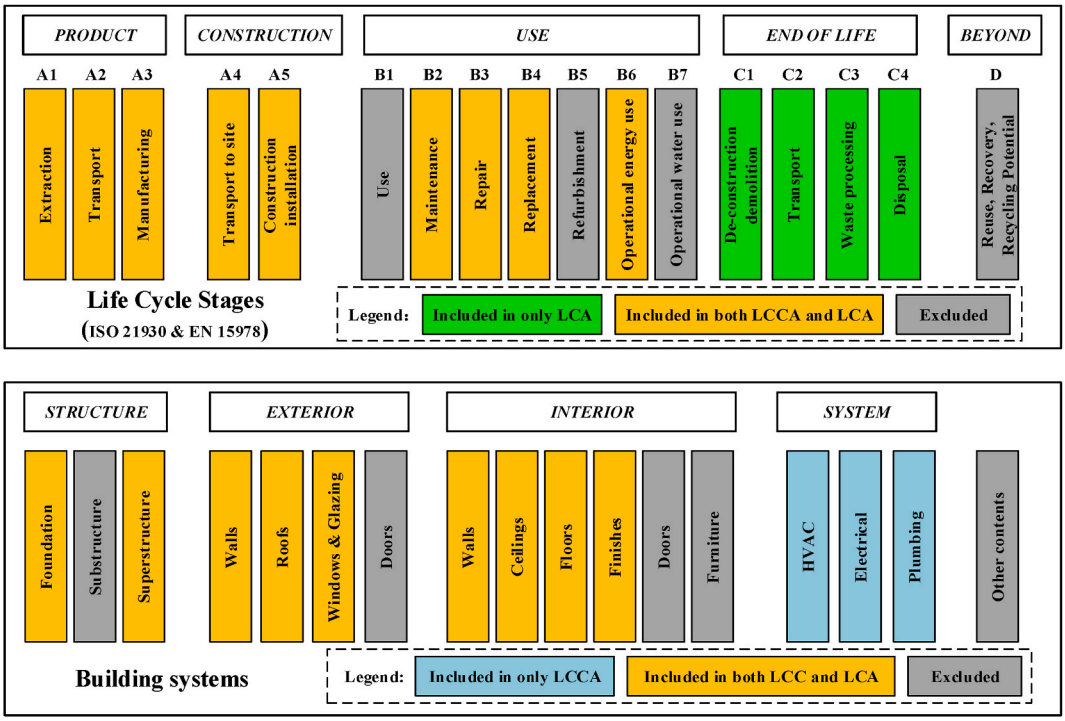

Fig. 7. Scope of included life cycle stages and building systems.

conduct LCA for the whole building. The Athena takes into account the environmental impacts of all life cycle phases of a building, except those caused by earthquakes. And the USA average data is used for both sites.

3.3. Loss analysis under seismic hazard

3.3.1. Structural modeling

The design of the moment frames in the two orthogonal directions is identical according to FEMA 355C [56]. Thus, only the structure in the NS direction is considered. 2D finite element models are modeled using the nonlinear dynamic analysis program OpenSees [61] to simulate the dynamic response of two structures under seismic hazards. The schematics of both numerical models are shown in Fig. 8 (b) and (c). Details of the components are all consistent with the corresponding research of the MRF [58] and SCBF [57, 59]. The nominal strength of beams and columns in both frames is 248 MPa (36 ksi) and 345 MPa (50 ksi), respectively. The gravity load is added on the leaning column to capture the P-Delta effect. A 5% Rayleigh damping associated with the first and third vibration modes is considered.

The beams of simply connected bays are modeled with truss elements for both models. All other beams and columns are modeled using a single elastic element with rotational springs at both ends. The modified Ibarra-Medina-Krawinkler (IMK) model [62] is adopted to capture the deterioration behavior of beams and columns. Parameters associated with IMK are determined according to Ref. [63].

As for each brace in the SCBF, ten force-based elements with fiber sections are used to capture the mechanical behavior steadily. Initial imperfection based on a half-sine wave distribution is added to capture the right global buckling behavior of braces, and the maximum deflection is set as 0.1% of the effective length of the brace. Rotational springs with Steel02 material are used to model the brace gusset connections. To replicate the extra constraints supplied by gusset plates on beam-column connections, rigid links are used. By comparing with the original research results, the accuracy of the first three natural periods and vibration modes of the numerical model is verified.

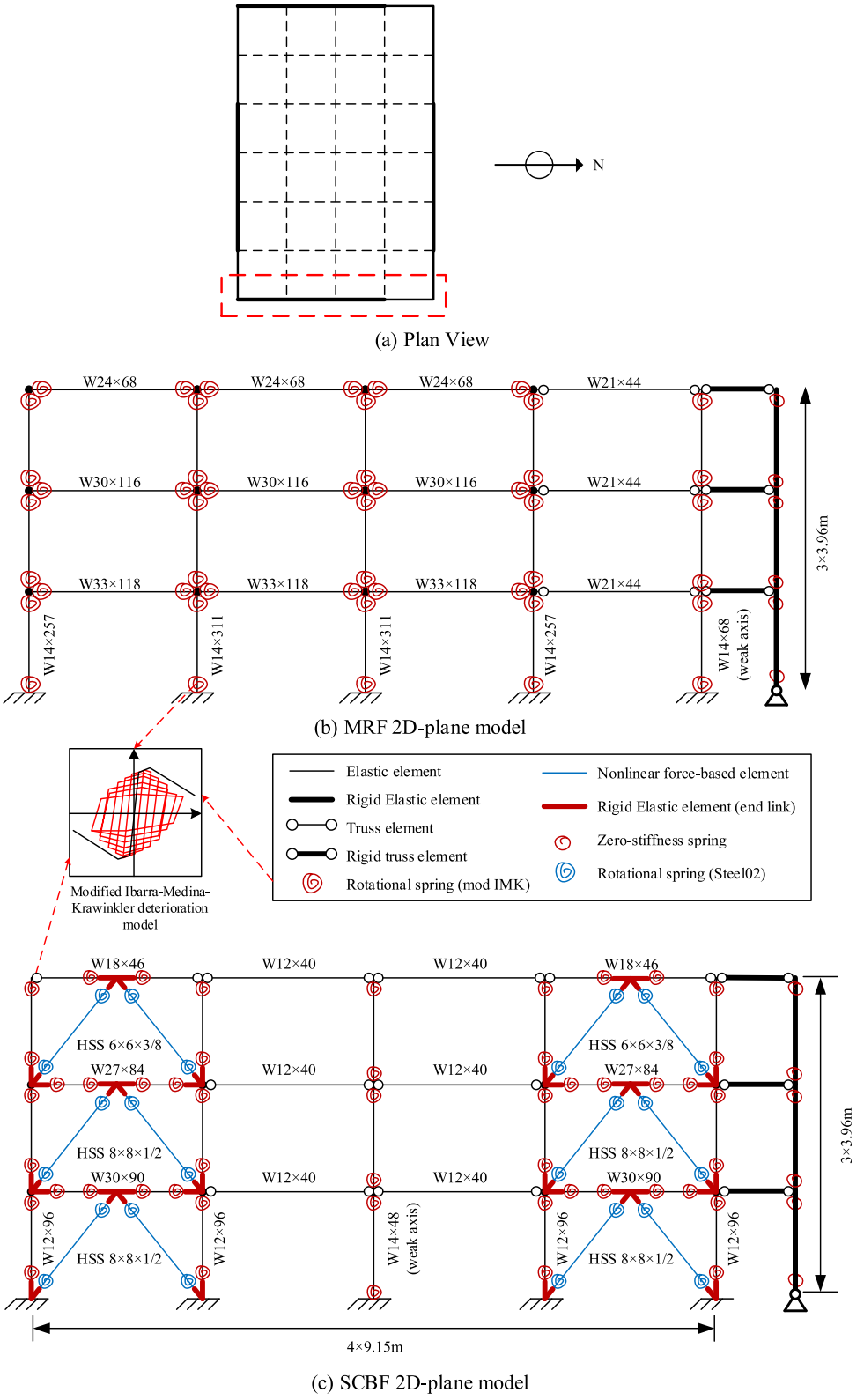

Fig. 8. Information on building structure models.

3.3.2. Hazard analysis

Hazard analysis identifies the seismic hazard at a specific site. In this study, a series of LA's and Boston's hazard curves were obtained with the USGS website tool by the given building location and site class, as shown in Fig. 9. The hazard curve at the specific structure's fundamental period is determined by linear interpolation, due to limited periods provided on the website.

A suite of suitable IMs is the basis for subsequent analysis. Therefore, it's desirable to select a rational range of ground motion exceedance frequencies and corresponding spectral accelerations. According to the recommendation of FEMA P-58, a range of exceedance frequencies is deemed appropriate if it is associated with a range of IMs that are anticipated to cause building damage ranging from minor to total destruction. In this study, the minimum and maximum spectral acceleration ($S_a^{\min}$ and $S_a^{\max}$) were set to 0.05 g and 2.05 g, respectively. And then, see Fig. 10, the hazard curve within this range was split into eight equal intervals. The IM used for subsequent analysis is the midpoint spectral acceleration for each interval. And the annual occurrence probability corresponding to each IM is the difference between the mean annual frequencies of exceedance at the endpoints of the interval. Table 4 shows the selected IMs and corresponding annual occurrence probabilities.

3.3.3. Structural analysis

Structural analysis identifies the building's responses to given ground motions. The distributions of EDPs at each IM and the collapse fragility of considered structures, which are both used for subsequent damage and loss analysis, are expected to be obtained from IDA.

In the IDA, the far-field ground motion set provided in FEMA P695 [64] is selected, which consists of 22 pairs, with just one component from each pair chosen. To acquire precise residual displacements of the structures, 30 s of damped free vibration history are appended after each ground motion's original time history. The $S_a(T_1)$ (T_1 is 1.0 s for MRF model and 0.4 s for SCBF model) of the 22 ground motions selected are scaled to the spectral acceleration of the corresponding intensity level. Then, in IDA, at each IM, the nonlinear time history analyses are performed using scaled ground motions.

The collapse fragility of considered structures must be assessed to determine whether the building is repairable or irreparable in each realization. The corresponding probability of collapse at each intensity level can be obtained from IDA. As for judging whether the collapse occurs or not from an IDA curve, according to Vamvatsikos and Cornell, collapse is determined by the following three rules, whichever first be satisfied: 1) IM-based rule, i.e., the slope of the IDA curve falls below 0.2 times the original slope, 2) Damage Measure (DM) based rule, i.e., the PIDR exceeds 0.1. Finally, as shown in Fig. 11, the IDA results are fitted with lognormal cumulative distribution function to construct the collapse fragility curves.

After getting the original demands matrix from Eq. (7) is used to generate 10,000 simulated *EDPs* at each intensity level. Besides, the generation process considers the effect of modeling uncertainty, β_m. The modeling uncertainty is related to two factors, i.e., construction quality, β_c, and the nonlinear analysis model quality, β_q. Thus, β_m can be estimated according to:

$$\beta_m = \sqrt{\beta_c^2 + \beta_q^2} \tag{21}$$

According to FEMA P-58 recommendation [12], when the two factors are all considered to be average quality, the β_c and β_q are both set as 0.25. Hence, β_m is estimated to be 0.35.

3.3.4. Seismic loss estimation

The earthquake-induced impact assessment methodology and the data used in this paper were adopted from the FEMA P-58 [12] documentation and the detailed fragility data provided therein. The FEMA P-58 fragility database provides probability distributions of various "loss" required to repair the damaged components. The earthquake-induced impacts, including the economic loss, GWP, PEU, casualties and downtime, are evaluated based on component-level time-based assessment in this section. The economic loss, GWP, PEU

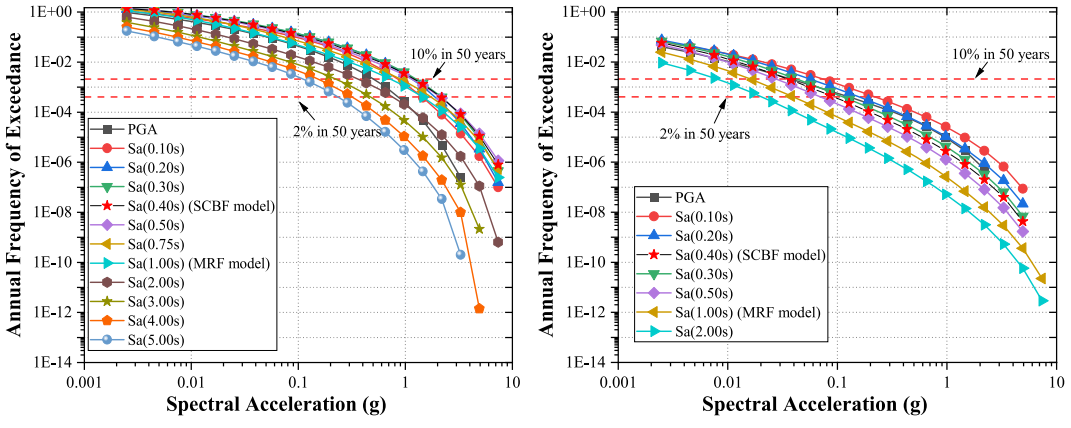

Fig. 9. Hazard curves.

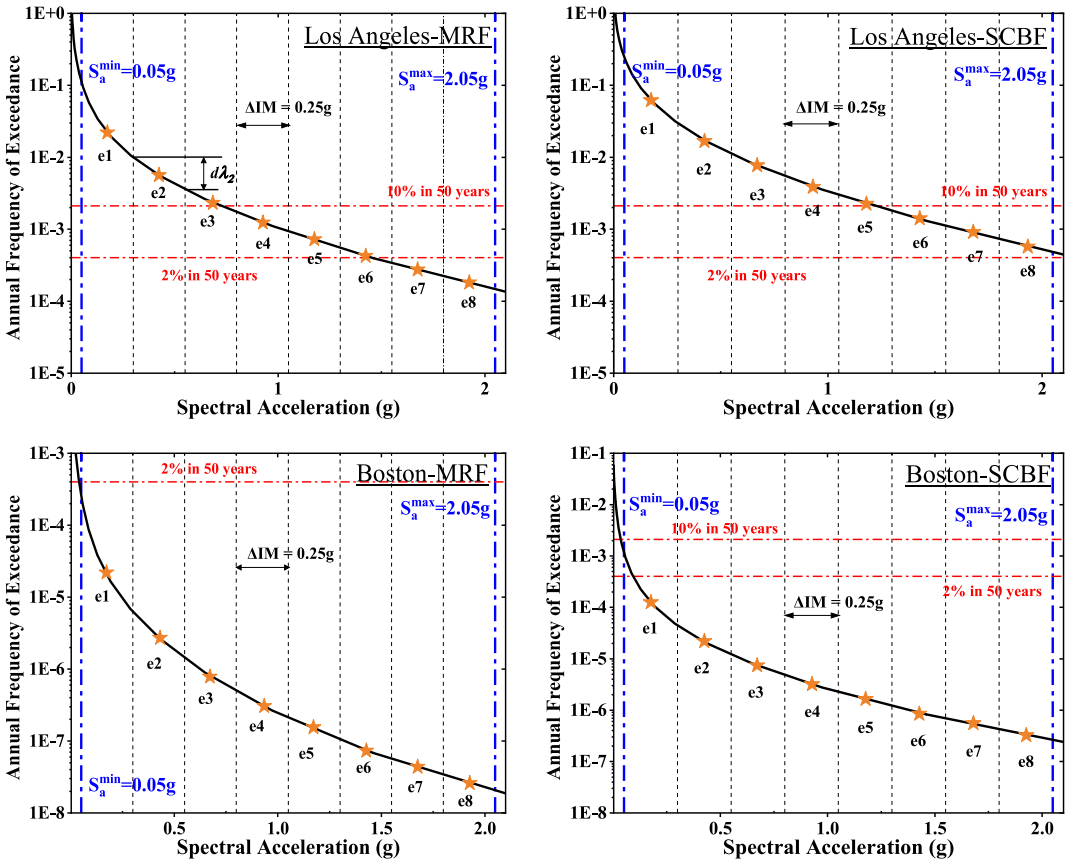

Fig. 10. Hazard analysis.

Table 4
The hazard analysis results.

Site	Earthquake intensity no.	Spectral acceleration (g)	Annual probability of occurrence ($\Delta\lambda$)	
			MRF	SCBF
Los Angeles	e1	0.175	1.03E-01	2.18E-01
	e2	0.425	6.25E-03	1.81E-02
	e3	0.675	2.01E-03	6.05E-03
	e4	0.925	9.12E-04	2.81E-03
	e5	1.175	3.60E-04	1.16E-03
	e6	1.425	2.65E-04	8.54E-04
	e7	1.675	9.66E-05	3.18E-04
	e8	1.925	9.65E-05	3.18E-04
Boston	e1	0.175	2.78E-04	1.23E-03
	e2	0.425	4.83E-06	3.21E-05
	e3	0.675	1.08E-06	8.15E-06
	e4	0.925	3.66E-07	3.10E-06
	e5	1.175	1.01E-07	1.01E-06
	e6	1.425	7.10E-08	7.21E-07
	e7	1.675	1.82E-08	2.13E-07
	e8	1.925	1.82E-08	2.13E-07

are calculated as the summation of repair cost, GWP, PEU of all structural, nonstructural components and contents. The replacement cost, GWP, PEU is assumed to be 1.25 times the construction cost, GWP, PEU. The downtime is reflected by the total repair time of a damaged building, which is estimated based on each component's repair time and the maximum number of workers per square foot for repair (assumed to be 0.002 in this paper) [12]. Serial repair strategies are considered for downtime analyses, which assume work occurs sequentially between floors. Referring to the example provided by FEMA P-58, the replacement time is assumed to be 431 days. For assessing the number of casualties, a building population model is adopted from FEMA P-58 recommendation for commercial offices, which describes the number of people present in the building by occupancy, time of day, day of the week, and month of the year

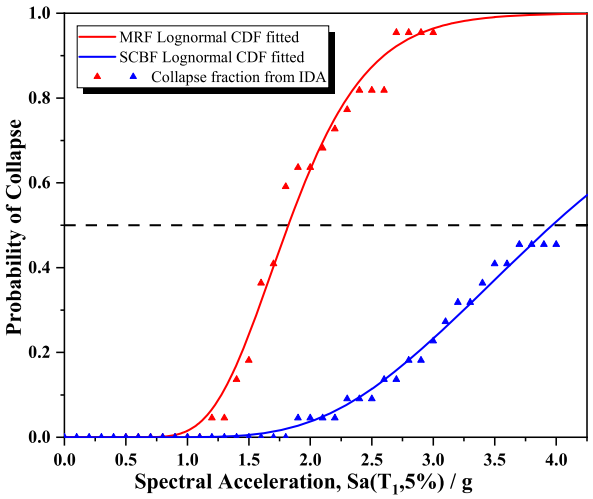

Fig. 11. Collapse fragility curve.

[12].

The loss estimation is performed in Python program together with the fragility data provided in FEMA P-58 and relevant literature [16]. Appendix Table A3, A4 summarizes the information about structural and nonstructural components considered in loss estimation. Fig. 12 shows the seismic economic loss of both MRF and SCBF under different IMs when the envelope is GCW. Each loss curve generally resembles a three-fold line. The economic loss before the "turning point" is caused by the repair cost for damaged components in repairable "realizations". Since the replacement cost in this paper adopts a determined value, the loss curve goes into a plateau stage until the replacement cost is reached. With the increase of IM value, the probability of the loss value reaching the replacement value gradually increases. This is not only caused by the increased probability of collapse, but also by the large residual deformation caused by the large IM resulting in a large probability of failure to repair. Compared with MRF, SCBF's obviously excellent anti-collapse ability and anti-lateral force ability make the economic loss of SCBF under all considered earthquake intensities significantly smaller than that of MRF.

The probability of exceedance of loss in 50 years can be determined by the time-based loss analysis introduced in Section 2.2.2, as shown in Fig. 13. Figs. 14–18 shows all results from the time-based assessment. It can be seen from the economic loss curve that although the initial construction cost of GCW is higher than that of EIFS, its seismic fragility is better, and its seismic performance in the stage with a higher occurrence probability is better than that of EIFS. Similar findings are found for the other metrics assessed. Note that the performance gap caused by the different fragility of different envelope systems can be compensated by a more efficient resistant structure system. For MRF, the gap caused by fragility is quite obvious, but the gap narrows significantly on SCBF. All results show that the seismic performance of SCBF is better than that of MRF. Unlike other metrics, the number of casualties is mainly caused by the fall of nonstructural components and the collapse of the buildings. In addition, the discrete population model also leads to a different shape of the number of casualties than others, which is not the classical "three-fold line".

All curves show that SCBF outperforms MRF, which also indicate the importance of the resilience structure study. However, it is important to emphasize here that seismic-enhanced structures do not mean the optimal scheme, which needs to be determined in the context of local conditions. Although the SCBF structure in this paper is well designed to obtain better seismic performance than MRF

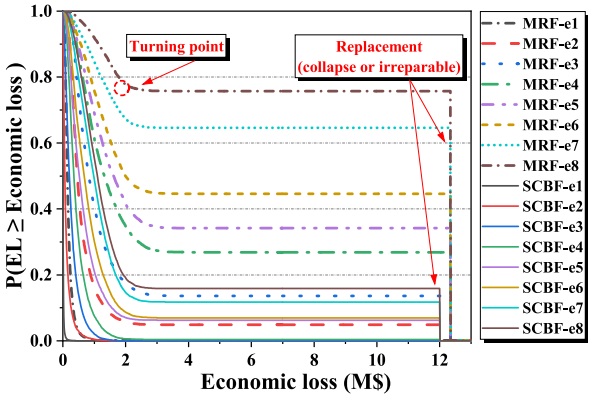

Fig. 12. The seismic economic loss of MRF and SCBF under different IMs.

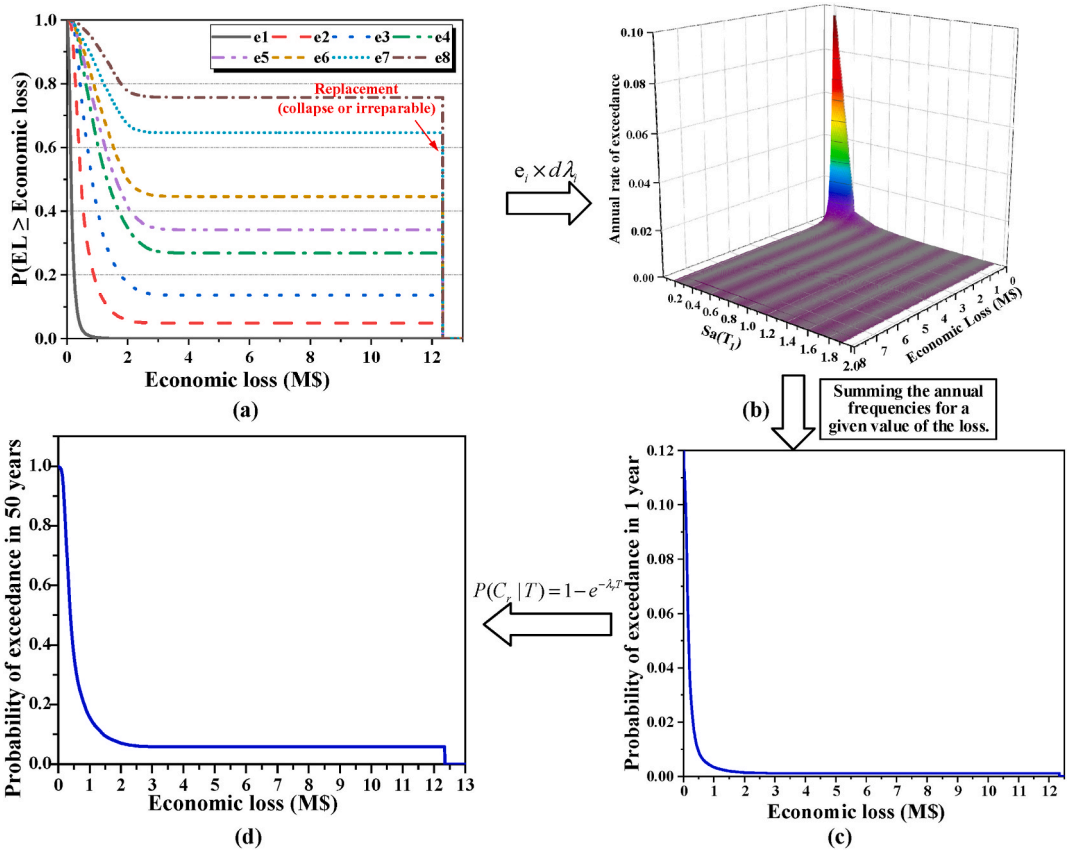

Fig. 13. Time-based loss analysis: a) seismic economic loss under different IMs, b) annual rate of exceedance under different IMs, c) probability of exceedance in 1 year, d) probability of exceedance in 50 years.

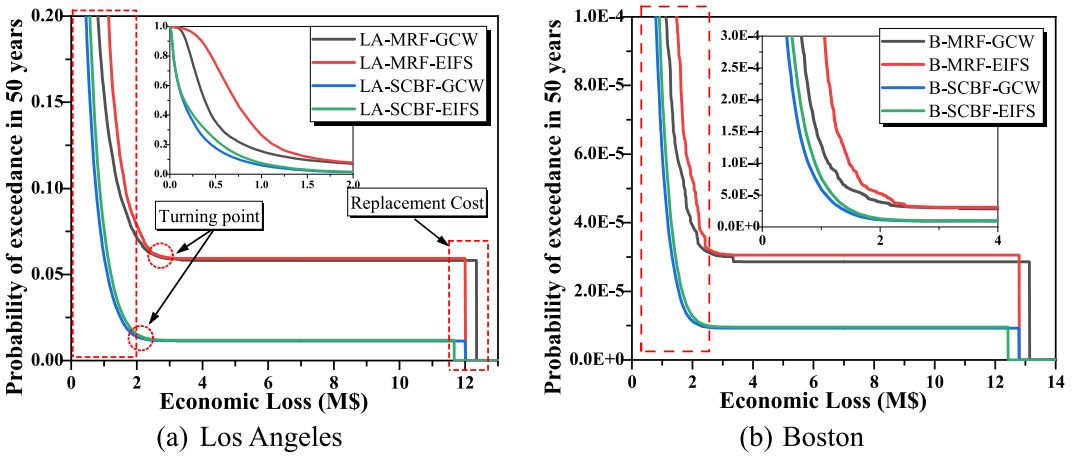

Fig. 14. Economic loss.

with less steel use, the implementation of many existing seismic-enhanced structures is generally accompanied by more material usage to increase the redundancy of structural safety. This redundancy may be reasonable in a more seismically active area like Los Angeles, but in a location like Boston, where the probability of an earthquake is extremely low, the redundancy may be less meaningful or even unsustainable.

3.4. Building energy modeling

In this section, the whole building energy modeling is conducted to quantify the economic cost, GWP, and PEU during the

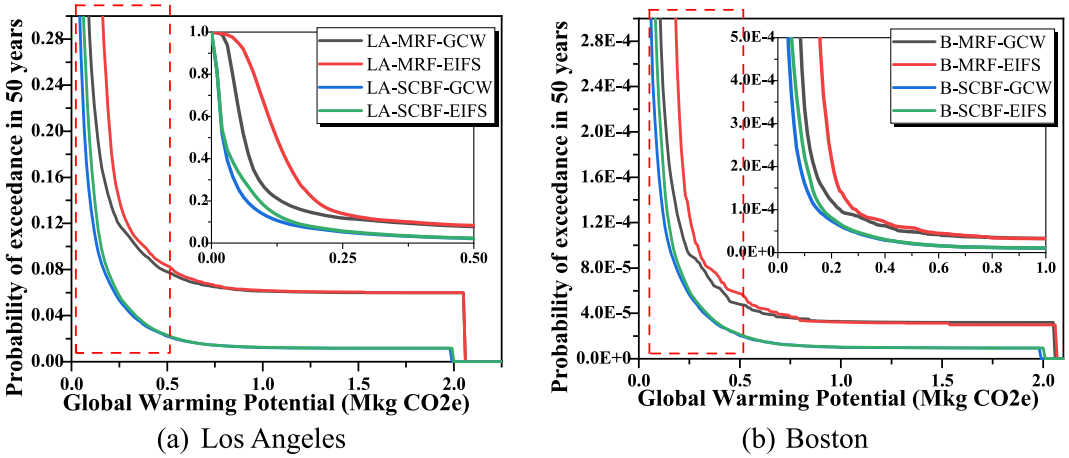

Fig. 15. Global warming potential.

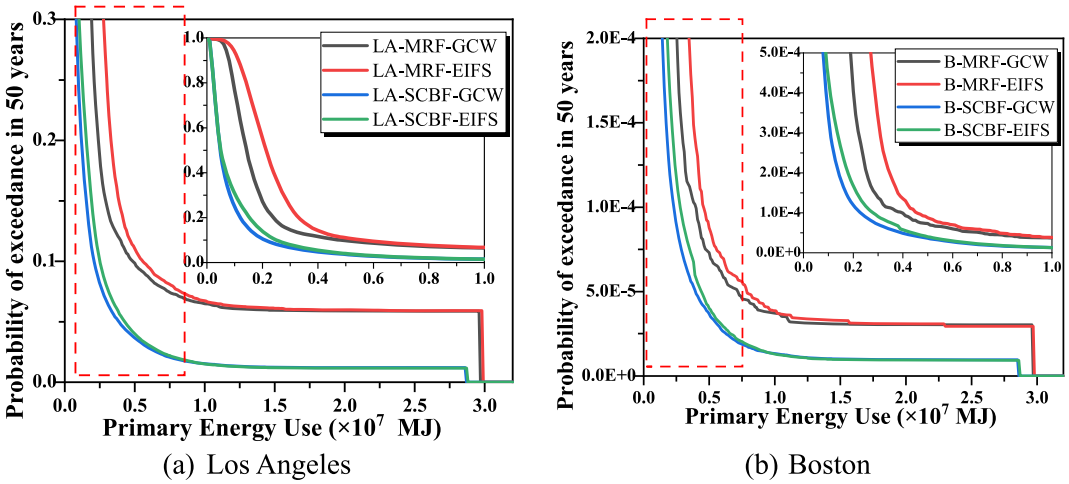

Fig. 16. Primary energy use.

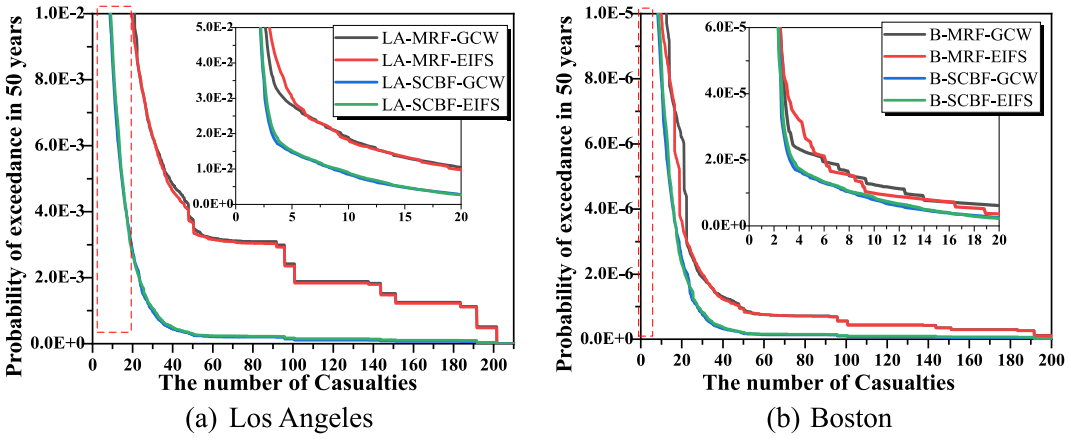

Fig. 17. The number of casualties.

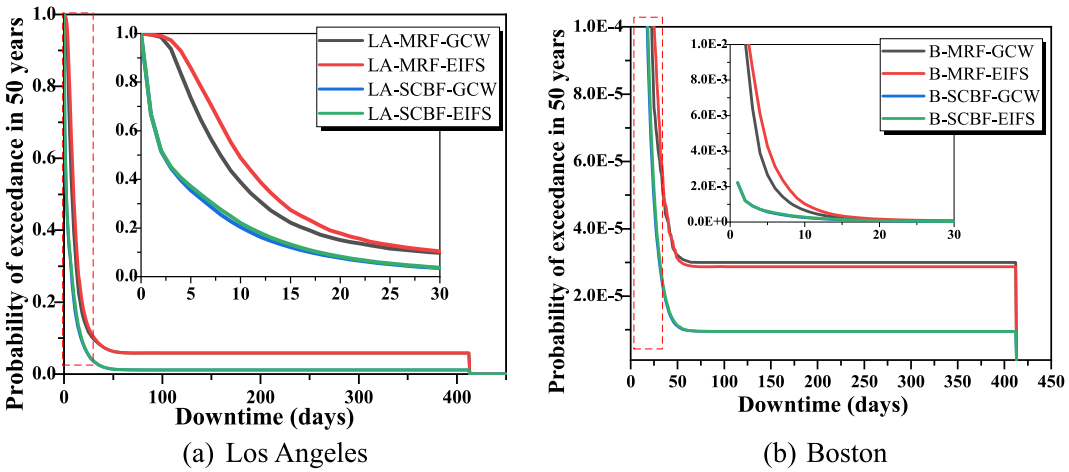

Fig. 18. Downtime.

operational phase. Based on the column layout, five thermal zones are assigned to each floor, see Fig. 19 (a). The model settings, such as occupancy, office equipment, and HVAC, are set with reference to the prototype medium office building developed by the US Department of Energy. For HVAC, the variable air volume reheat system is adopted, which uses electricity and natural gas for cooling and heating, respectively. The thermostat setpoints for cooling and heating are 75℉ and 70℉, respectively. And the thermostat setback for cooling and heating are 80℉ and 60℉, respectively. Building energy model is established by SketchUp and OpenStudio (as shown in Fig. 19 (b) and (c)), and converted to EnergyPlus input file IDF format. To consider the uncertainty of the parameters in BEM, three parameters that are deemed to have a possible non-negligible impact on energy simulation are assumed to have some uncertainties. Their mean values are referred to the recommendations of the DOE prototype building, and the variances are referred to existing studies [18], as listed in Table 5.

500 simulations are performed for each alternative, and the electricity and natural gas consumption for each simulation is extracted and then converted into cost, GWP, and PEU using local electricity prices and Athena. Note that the three considered parameters in Table 5 are the same for all alternatives in each simulation. From the result of 500 simulations, as seen in Fig. 20, the operational phase accounts for a high percentage of the whole life cycle, about 75–90%, which is consistent with existing research. The high dispersion of

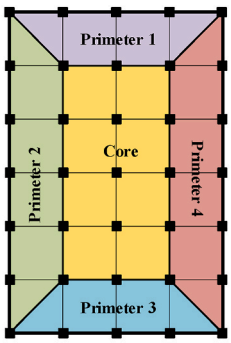

(a) Thermal zones of building archetypes.

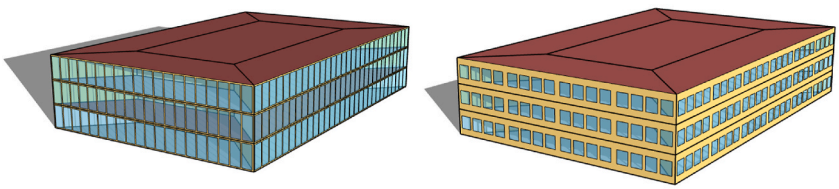

(b) GCW model (c) EIFS model

Fig. 19. Building energy modeling.

Table 5
Normal distribution characteristics of input parameters.

Parameter	μ	σ (%)
Occupancy, person (people/m^2)	0.05382	25
Lighting density (W/m^2)	9.6875	10
External window U-value (W/m^2K)	1.2	10

the outcome emphasizes the necessity to consider the uncertainty of the building energy modeling. Compared with LA, Boston's cold climate brings more natural gas demand and therefore more economic and environmental impacts, especially the global warming potential. High-performance envelope like EIFS with vacuum insulation panel helps reduce this impact.

3.5. Multi-criteria decision-making

Decision-makers are expected to be experts with experience in sustainable and resilient building design, because too many factors are related to the selection of design alternatives. However, such comprehensive experts are rare. This paper uses the opinions of 16 researchers or engineers in relevant fields corresponding to the resilience and sustainability aspects, half of them are engaged in resilient steel structure design and the other half are engaged in sustainable building design. Firstly, each decision maker individually carries out pairwise comparisons by being asked questions such as "Compared with criterion C_1, how important do you think C_2 is?". For example, if the decision maker thinks C_2 is strongly important, then the answer is 5 according to Table 1. But if the reverse is true, the number is 1/5. Then, there are 16 values for each array of the pairwise matrix. Following step 1–7 mentioned in Section 2.3.1, 10,000 sets of subjective weights can be obtained. Fig. 21 shows the statistical histogram of each criterion. The variance and mean of weights for the criteria are given in Table 6. The emphasis on people's safety is well recognized as the original purpose of the building design, and as such it receives the relatively highest weighting. The distribution shows that it retains the opinions of different experts. Hence, compared with the traditional method, the method used in this paper can better deal with the various preferences among multi-disciplinary experts.

10,000 evaluation matrices are generated from the result of performance assessment. EWM objective weights and composite weights are calculated following step 8–11 in weight calculation process. Note that in this paper, in the process of sampling from the performance assessment's outcome, the impacts of the earthquakes are sorted from minimum to maximum, and then a random number is used to extract a group from them. Similarly, for the operational phase calculation results, the results of all alternatives from one of the simulations are sampled as the input to an evaluation matrix. The sampling process described above (as illustrated in Fig. 22) ensures that unrealistic situations do not arise, such as small economic losses accompanied by long downtime, etc. It also ensures that the envelope systems are compared for the same given load and glass parameters. The result of each evaluation is determined through the process mentioned in Section 2.3.2.

In each evaluation, the relative closeness (i.e., S_i) calculated by Equation (20) in TOPSIS method described in Section 2.3.2 is called "score" here. The larger the score, the more ideal the solution. As shown in Fig. 23, the distribution of the scores for each alternative shows approximate alternative ranking, but the dispersion cannot be ignored. Remarkably, the distribution of scores in the Boston area will have a small tail distributed at locations larger than the wave crest, while the vice versa is the case in LA. Obviously the different seismic activity levels cause this result. For instance, the score distribution of SCBF-EIFS-LA shows a high probability of receiving the highest score due to smaller energy demand and lower labor and construction costs in the LA region. However, it also has a non-negligible probability of obtaining a small score due to the instability caused by the combination of the high seismic intensity of the LA and the vulnerability of the EIFS. In comparison, although the wave position of the distribution of SCBF-EIFS in Boston is located after LA, its scores get higher in some cases. This is because the minor seismic activity in Boston results in a low impact from earthquakes, allowing for a higher score when the LA scenario suffers seismic damage. The results presented above demonstrate the effectiveness of the proposed framework in capturing the variability that arises from different seismic levels, climatic conditions, structural systems, and envelope systems.

Fig. 24 illustrates the results of ranking the 4 alternatives for each location separately. In this paper, the operational phase dominates the whole life cycle. Therefore, the better the performance of the envelope system closely related to the operation phase, the higher the ranking of the alternative, as seen in Fig. 24 (a). Due to the characteristics of the cases studied in this paper, SCBF-EIFS takes the first place with absolute advantage, while MRF-GCW is the opposite. For alternatives in Boston, the difference between the seismic resilience of MRF and SCBF has little effect on the results. But for alternatives in LA, there is close to 9% probability that GCW with SCBF exceeds EIFS with MRF. In other words, the proposed method gives the "reliability index" of the alternative ranking. In practice, when a designer improves the alternative based on the results of the analysis, it can be re-ranked and the change in reliability index can judge the degree of merit of the improvement measures.

Typically, as the service life increases, the impact of the operational phase becomes a higher percentage of the total life cycle. However, Fig. 24 (b) shows that when the studied service life is increased from 50 to 100 years, there is minimal change in decision-making in the low-earthquake region, but a significant change in the high-earthquake region, where the probability of ranking higher for less resilient building solutions decreases. This has to do with the importance decision-makers place on life safety. The longer the service life, the higher the probability that the building will experience an earthquake during its life cycle. Therefore, more attention should be paid to the resilient design of buildings with long service life. Although the operational phase is crucial in studied cases, in recent years, many studies and practices, dedicated to designing ultra-low energy or net-zero energy buildings, have greatly reduced the impact of the operational phase. Fig. 24 (c) shows the decision-making when the impact of the operational phase is assumed to be

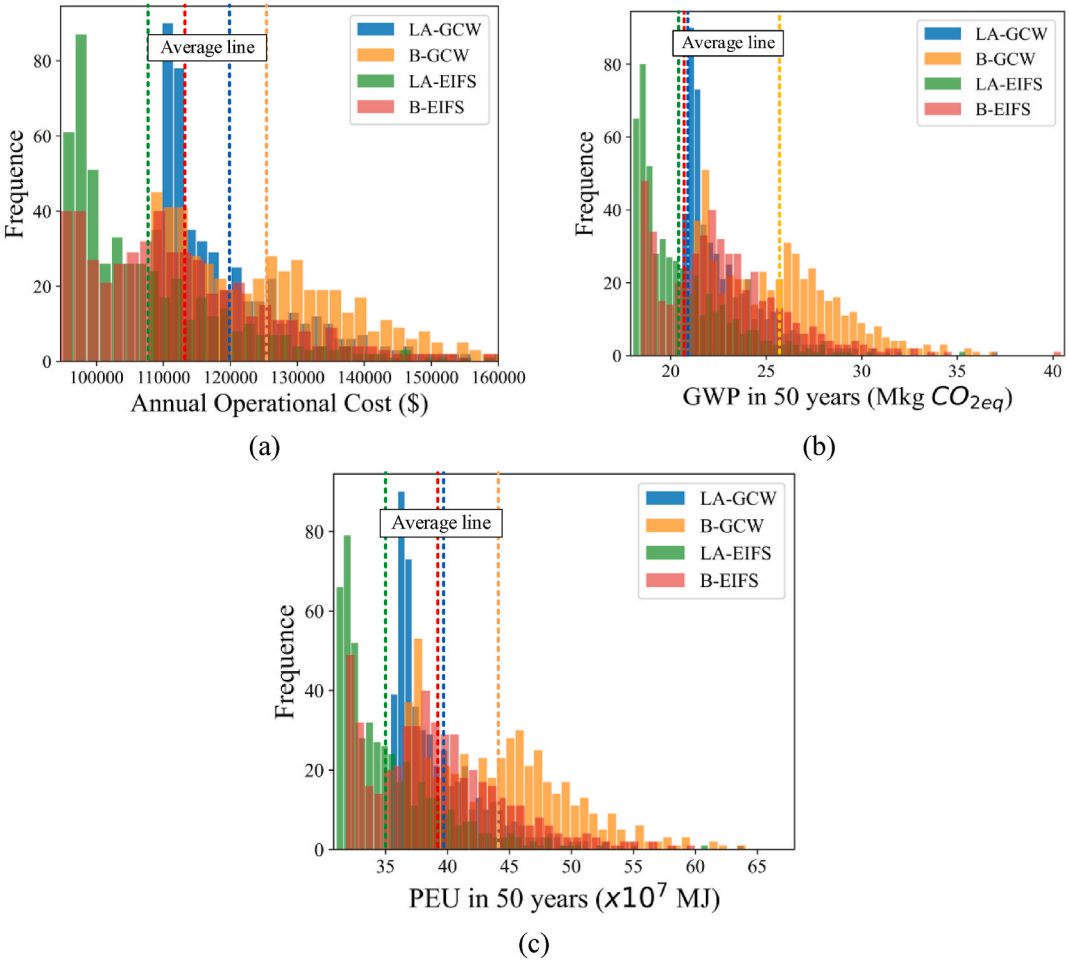

Fig. 20. Impact of operational phase: a) annual operational cost, b) GWP in 50 years, c) PEU in 50 years.

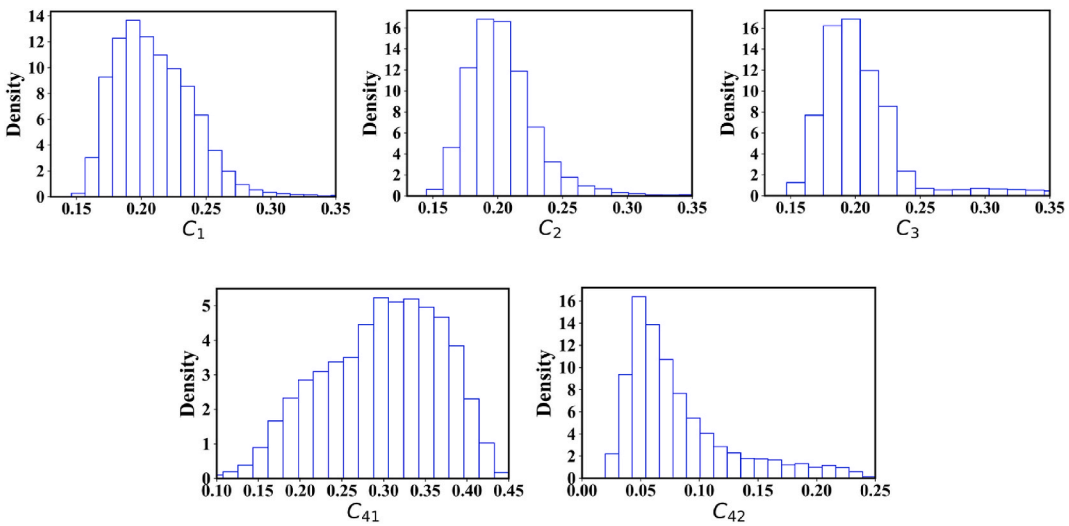

Fig. 21. Statistical histogram of each criterion.

Table 6
Variance and mean of weight for the criteria.

Criterion	Mean of weight	Variance (10^{-2})
C_{11}	0.210	2.98
C_{12}	0.203	2.72
C_{13}	0.206	3.76
C_{21}	0.298	7.02
C_{22}	0.082	4.62

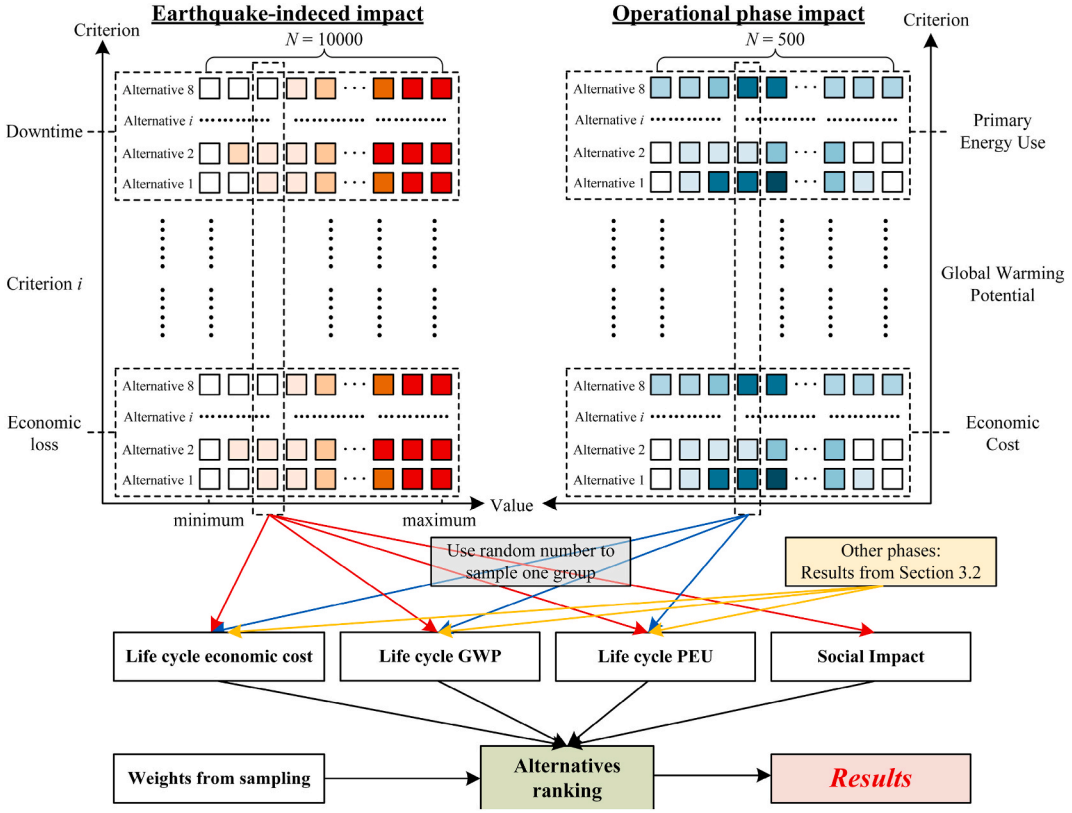

Fig. 22. Sampling process in this paper.

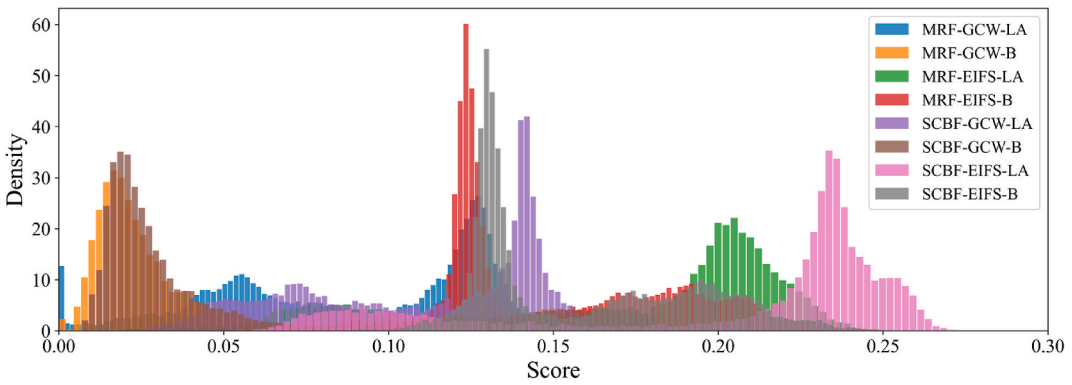

Fig. 23. Scores distribution of each alternative.

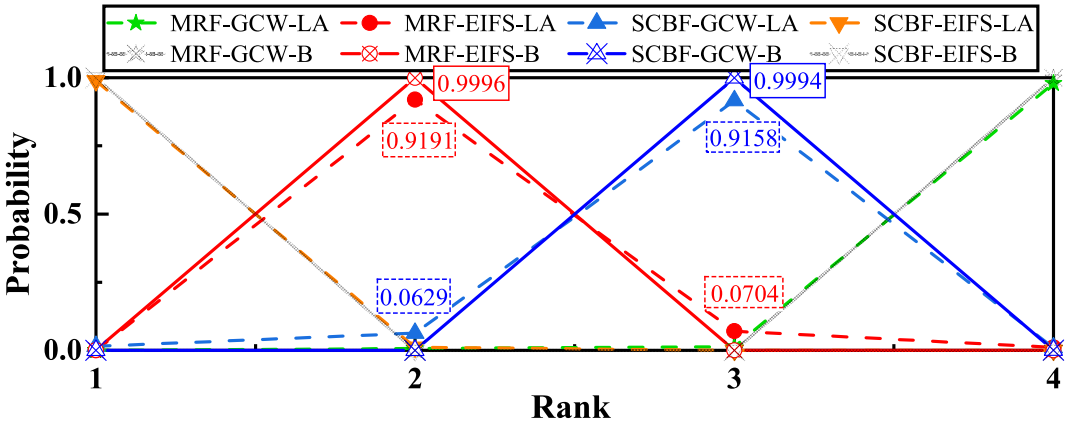

(a) 50 years.

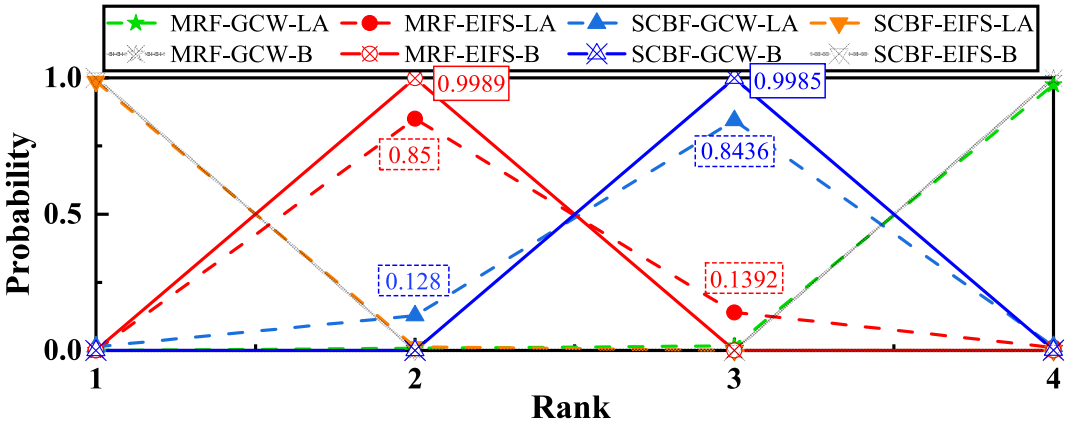

(b) 100 years.

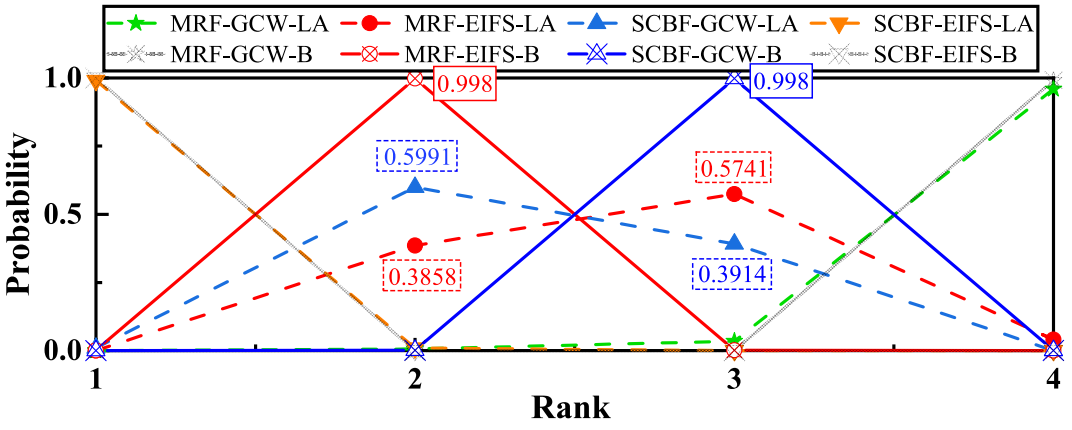

(c) 50 years (Assume that the impact of operational phase is reduced to 5%).

Fig. 24. Rank results for 4 alternatives in LA and Boston, respectively.

reduced to 5%. At this point, the decision in the low-earthquake region is dominated by the envelope system as usual, while the high-earthquake region shows the opposite result. This reveals that the influence of the resilience of the structural system on the ranking of low-energy building solutions in high-earthquake regions is extremely significant. Note that this observation will be more noticeable in real situations since low-energy buildings tend to require higher economic inputs and also incur more losses when faced with earthquakes.

4. Summary and conclusions

This research proposed a novel probabilistic MCDM framework to support the selection of design solutions from a resilience and sustainability perspective, holistically considering the building's life cycle cost, global warming potential (GWP), primary energy use (PEU), and social impact. The proposed framework outlines a systematic process of solution selection based on the life-cycle concept, aiming to evaluate the seismic performance and environmental impact, and find the near-optimum design solutions. Specifically, time-based seismic performance assessment methodology in the advanced PBEE-2 and building energy simulation considering uncertainties are embedded within the life cycle analysis of buildings. Besides, a novel MCS-MCDM method was developed to provide support for more robust decision-making in solutions selection. The proposed method was illustrated through the case studies of 3-story medium-sized archetype office buildings located in regions with instinct seismic risks and climate conditions, i.e., Los Angeles, CA, and Boston, MA. The case studies show that the proposed framework not only integrates several different assessment criteria, but also can effectively propagate multiple uncertainties (e.g., experts' opinions, seismic loss estimation, energy modeling) to the final decision outcome to improve its robustness. In addition, the framework shows potential to be further extended to consider more criteria and applied to other decision scenarios (e.g., the selection of low carbon building solution, long lifetime building solution).

Main conclusions are drawn below:

- The proposed framework captures the different preferences of decision-makers while considering geographical locations to holistically design buildings' structural and envelope systems. Compared with the traditional decision-making methods, it can provide more information to facilitate robust decision-making by considering various sources of uncertainties in building seismic analysis and building energy simulation.
- The combination of AHP and Monte Carlo simulation effectively preserves the different preferences of the experts by generating multiple groups of subjective weights from the experts' original opinions. In the case studies, the high degree of dispersion exhibited by subjective weights emphasizes the sensitivity of criteria weights to experts' preferences.
- The whole building energy simulation considering uncertainties is recommended to be integrated into the holistic design framework. While this study only considered uncertainties associated with three parameters, the result dispersion indicates that building energy performance is sensitivity to several parameters of buildings such as envelope properties and internal loads. Therefore, using only deterministic values in decision-making may lead to misleading results.
- In the alternative ranking process, the special concentrically braced frame (SCBF) shows better economic and seismic performance over the moment-resisting frame (MRF), owing to its seismic-resistant design. Buildings with SCBF have better seismic resilience with less material usage.
- For both studied locations (Boston, MA and Los Angeles, CA), the exterior insulation and finishing system (EIFS) with SCBF was found the most advantageous alternative, followed by EIFS with MRF. EIFS takes the top two places by a significant margin due to its superior energy performance, while the impact of the operational phase dominates the whole life cycle. This observation seems unassailable in Boston. But in Los Angeles, high seismic risk can cause a reduced rank of high-performance envelope alternatives, as evidenced by a reduction in the probability of a higher ranking.
- In high seismic regions, with the service life increasing from 50 to 100 years, the preferred design solutions favor those with higher seismic resistance. This is due to the fact that experts tend to give higher importance to life loss in this study's survey.
- For buildings with lower energy consumption but located in high seismic intensity regions, the building's seismic resilience outweighs operational energy performance and dictates the decisions.

The proposed procedure can be enhanced further, e.g., by embedding the site-specific weather uncertainties and climate change variability within BEM, by accounting for the uncertainties of the data used in LCC and LCA, by considering more regional differences (such as the different transportation assumptions and local electricity grids. Note that resilient and sustainable building design is still a fast-developing field. In future study or practice, a comprehensive industry database is needed to be established to accommodate a progressively more integrated architectural design framework. Collaborative efforts from multi-disciplinary teams are encouraged to incorporate more uncertainties into the proposed frameworks, such as those in LCA and LCCA. The combination of the proposed framework with new technologies, e.g., Building Information Model (BIM), is also needed and can be easily applied in practice [13, 65–67].

Authorship contributions

Jiajun Du: Conceptualization, Investigation, Methodology, Software, Validation, Formal analysis, Data curation, Visualization, Writing – original draft.

Wei Wang: Conceptualization, Resources, Project administration, Funding acquisition, Supervision, Writing – review & editing.

Ting Lou: Software, Writing – review & editing.

Hongyu Zhou: Conceptualization, Writing – review & editing.

Declaration of competing interest

The authors declare that they have no known competing financial interests or personal relationships that could have appeared to influence the work reported in this paper.

Data availability

Data will be made available on request.

Acknowledgment

The financial supports from the National Natural Science Foundation of China (NSFC) with Grant No. 51820105013 and National Key Research and Development Program of 14th Five-Year Plan of China with Grant No. 2022YFC3801904 are gratefully acknowledged. This study is also supported by the Top Discipline Plan of Shanghai Universities-Class I with Grant No. 2022-3-YB-18 and Shanghai 2022 Science and Technology Innovation Action Plan Social Development Science and Technology Research Project with Grant No. 22dz1201700.

Appendix

Table A1
Building components considered in case studies and corresponding data in brief.

Category	Component	Quantity	Initial Construction Cost ($/m^2) LA/Boston	Annual Maintenance Cost ($/m^2) LA/Boston	Life cycle GWP ($kgCO_2$/m^2)	Life cycle PEU (MJ/m^2)
Substructure	Strip footing, reinforced, 12″deep x 24″ wide	183 m	4.09/4.47	–	2.48	23.42
	Spread footing, 3000 PSI, 6'square x 20″deep	123 EA	17.11/18.70		12.34	88.70
	Spread footing, 3000 PSI, 7–6″square x 25″deep	13 EA	3.23/3.53		2.54	18.27
	Slab on Grade	2007 m^2	19.70/21.64		15.28	150
Shell	Floor: Metal deck with concrete slab + Fireproofing, gypsum board	6020 m^2	102.90/116.14	–	81.06	986.71
	Roof: Metal deck with concrete slab + Fireproofing, gypsum board	6020 m^2	34.34/38.64		27.02	328.90
	Envelope: GCW	2174 m^2	188.78/191.43	4.54/4.86	43.85	509.97
	Envelope: EIFS	2174 m^2	154.63/156.79	1.73/1.85	46.35	514.95
Interiors	Partitions: Gypsum board with metal studs	9420 m^2	59.09/59.92	5.56/5.95	33.23	894.24
	Partitions: Gypsum board with wallpaper	2007 m^2	13.89/14.09		1.78	28.38
	Floor Finishes: clay tile	6020 m^2	120.56/122.24		9.97	169.44
	Suspended ceiling Gypsum board ceiling	6020 m^2	44.02/50.59		4.15	64.78
Services	Plumbing Fixtures: Water closet, Lavatory, Water cooler, and etc.	Detailed quantities of "Services" can be found in Table A4 and Square Foot Estimator Tool provided by RSMeans Online.	38.32/40.69	1.85/1.98	–	–
	Standpipes		9.36/9.50			
	Rain Water Drainage: Roof drain		7.00/7.53	–		
	Domestic Water Distribution: Gas fired water heater		4.74/4.84	4.77/5.10		
	Air conditioner, offices, multizone		184.49/198.38			
	Sprinklers: Wet pipe sprinkler systems, steel		40.36/43.92	0.79/0.85		
	Electrical Service: Service/ Feeder/Switchgear installation		16.04/16.26	5.03/5.38		
	Lighting and Branch Wiring Receptacles incl plate, Miscellaneous power		138.64/151.66			
	Communications and Security: Telephone and		69.86/73.63			

(continued on next page)

Table A1 (*continued*)

Category	Component	Quantity	Initial Construction Cost ($/m^2) LA/Boston	Annual Maintenance Cost ($/m^2) LA/Boston	Life cycle GWP ($kgCO_2$/m^2)	Life cycle PEU (MJ/m^2)
	internet wiring, fire alarm systems					
Structure (Beams and Columns)	Table A2					
Fee	Contractor Fees		25% of ICC	–		
	Architectural Fees		7% of ICC	–		
Earthquake-induced	Table A3-A4, Figs. 14–18.					
Operational Phase	Fig. 20					

Note: EA – Each. ICC – Initial construction cost.

Table A2
Steel usage per unit building area for frames and corresponding data.

Components	Gravity Frames		MRF		SCBF		
	Beams	Columns	Beams	Columns	Beams	Braces	Columns
Steel Consumption(kg/m^2)	9.14	3.64	9.43	14.16	6.33	2.94	5.07
Economic Cost(dollar/m^2) LA/Boston	35.04/37.49	12.31/13.17	33.38/35.72	45.98/48.74	21.99/23.43	6.17/6.54	16.95/18.14
Global Warming Potential (kg CO_{2eq}/m^2)	9.62	3.84	9.93	14.90	6.66	5.02	5.33
Primary Energy (MJ//m^2)	174.4	69.42	179.37	270.72	120.91	80.72	96.83

Table A3
Structural components for one plane-frame considered in loss estimation.

Components	FEMA P-58 ID	EDP	Unit	Frame	Quantity per story		
					1st	2nd	3rd
Bolted shear tab gravity connections	B1031.001	PIDR	EA	MRF	2	2	2
				SCBF	4	4	8
Steel Column Base Plates, Column W < 150 plf	B1031.011a	PIDR	EA	MRF	1	–	–
				SCBF	5	–	–
Steel Column Base Plates, Column 150 plf < W < 300 plf	B1031.011b	PIDR	EA	MRF	2	–	–
				SCBF	–		
Steel Column Base Plates, Column W > 300 plf	B1031.011c	PIDR	EA	MRF	2	–	–
				SCBF	–		
Pre-Northridge WUF-B beam-column joint, beam one side of column, beam depth≥W30	B1035.042	PIDR	EA	MRF	2	2	–
				SCBF	4	–	–
Pre-Northridge WUF-B beam-column joint, beam both sides of column, beam depth≥W30	B1035.052	PIDR	EA	MRF	2	2	–
				SCBF	–		
Pre-Northridge WUF-B beam-column joint, beam one side of column, beam depth≤W27	B1035.041	PIDR	EA	MRF	–	–	2
				SCBF	–	4	–
Pre-Northridge WUF-B beam-column joint, beam both sides of column, beam depth≤W27	B1035.051	PIDR	EA	MRF	–	–	2
				SCBF	–		
Special Concentric Braced Frame, design to AISC minimum standards, Chevron Brace, Brace W < 40 plf	B1033.031a	PIDR	EA	MRF	–		
				SCBF	–	–	2
Special Concentric Braced Frame, design to AISC minimum standards, Chevron Brace, Brace 41 plf < W < 99 plf	B1033.031b	PIDR	EA	MRF	–		
				SCBF	2	2	–

Note: PIDR – Peak inter-story drift ratio.

Table A4
Nonstructural components considered in loss estimation.

Components	FEMA P-58 ID	Quantity per story	Fragility Unit of Measure	EDP	Story
Glass curtain walls*	–	725	1 m^2	PIDR	1–3
EIFS cladding*	–	725	1m^2	PIDR	1–3
Wall partition: gypsum with metal studs	C1011.001a	26	100 LF	PIDR	1–3
Wall partition: gypsum with wallpaper	C3011.001b	8	100 LF	PIDR	1–3
Suspended ceiling	C3032.001a	86	250 SF	PFA	1–3
"Services" related part (MEP system)					
Cold or hot portable-Small Diameter Threaded Steel	D2021.011a	0.91	1000 LF	PFA	1–3
HVAC Galvanized Sheet Metal Ducting-6 sq. ft	D3041.012a	0.43	1000 LF	PFA	1–3
HVAC Galvanized Sheet Metal Ducting less than 6 sq. ft	D3041.011a	1.62	1000 LF	PFA	1–3
HVAC Drops/Diffusers in suspended ceilings	D3041.031a	17	10 EA	PFA	1–3

(*continued on next page*)

Table A4 (*continued*)

Components	FEMA P-58 ID	Quantity per story	Fragility Unit of Measure	EDP	Story
Independent Pendant Lighting	C3034.001	628	1 EA	PFA	1–3
Variable Air Volume (VAV) box	D3041.041a	15	10 EA	PFA	1–3
Air Handling Unit Capacity:<5000CF	D3052.011a	4	4000 CF	PFA	1–3
Fire Sprinkler Water Piping	D4011.021a	5	1000 LF	PFA	1–3
Fire Sprinkler Drop Standard Threaded Steel	D4011.031a	2	100 EA	PFA	1–3
Low Voltage Switchgear	D5012.021a	1	225 AP	PFA	1–3
Motor Control Center	D5012.013a	3	1 EA	PFA	1
Cooling Tower	D3031.021a	3	75 TN	PFA	Roof
Chiller - Capacity: <100 Ton	D3031.011a	3	75 TN	PFA	Roof

Note: LF-Linear Foot, SF-Square Foot, CF-Cubic Foot, AP-Amp, TN-Ton, EA-Each, *-Data from Ref. [13]. PIDR-Peak Inter-story Drift Ratio, PFA-Peak Floor Acceleration.

References

[1] Global status report 2017, World green build Counc. https://www.worldgbc.org/news-media/global-status-report-2017. (Accessed 3 September 2022).
[2] LEED rating system | U.S. Green Building Council. https://www.usgbc.org/leed. (Accessed 10 November 2022).
[3] P. Bocchini, D.M. Frangopol, T. Ummenhofer, T. Zinke, Resilience and sustainability of civil infrastructure: toward a unified approach, J. Infrastruct. Syst. 20 (2014), 04014004, https://doi.org/10.1061/(ASCE)IS.1943-555X.0000177.
[4] P. Timmerman, Vulnerability, Resilience and the Collapse Ofsociety, 1981.
[5] A. Baird, A. Palermo, S. Pampanin, Façade damage assessment of concrete buildings in the 2011 Christchurch earthquake, Struct. Concr. 13 (2012) 3–13, https://doi.org/10.1002/suco.201100040.
[6] I. Kilanitis, A. Sextos, Integrated seismic risk and resilience assessment of roadway networks in earthquake prone areas, Bull. Earthq. Eng. 17 (2019) 181–210, https://doi.org/10.1007/s10518-018-0457-y.
[7] K.M. Mosalam, U. Alibrandi, H. Lee, J. Armengou, Performance-based engineering and multi-criteria decision analysis for sustainable and resilient building design, Struct. Saf. 74 (2018) 1–13, https://doi.org/10.1016/j.strusafe.2018.03.005.
[8] J.P. Chhabra, V. Hasik, M.M. Bilec, G.P. Warn, Probabilistic assessment of the life-cycle environmental performance and functional life of buildings due to seismic events, J. Architect. Eng. 24 (2018), 04017035, https://doi.org/10.1061/(ASCE)AE.1943-5568.0000284.
[9] Y. Dong, D.M. Frangopol, Performance-based seismic assessment of conventional and base-isolated steel buildings including environmental impact and resilience, Earthq. Eng. Struct. Dynam. 45 (2016) 739–756, https://doi.org/10.1002/eqe.2682.
[10] E. Asadi, A.M. Salman, Y. Li, Multi-criteria decision-making for seismic resilience and sustainability assessment of diagrid buildings, Eng. Struct. 191 (2019) 229–246, https://doi.org/10.1016/j.engstruct.2019.04.049.
[11] G.A. Anwar, Y. Dong, Y. Li, Performance-based decision-making of buildings under seismic hazard considering long-term loss, sustainability, and resilience, Struct. Infrastruct. Eng. 17 (2021) 454–470, https://doi.org/10.1080/15732479.2020.1845751.
[12] FEMA, Seismic Performance Assessment of Buildings, second ed., 2018.
[13] K. Angeles, D. Patsialis, A.A. Taflanidis, T.L. Kijewski-Correa, A. Buccellato, C. Vardeman, Advancing the design of resilient and sustainable buildings: an integrated life-cycle analysis, J. Struct. Eng. 147 (2021), 04020341, https://doi.org/10.1061/(ASCE)ST.1943-541X.0002910.
[14] V. Hasik, J.P.S. Chhabra, G.P. Warn, M.M. Bilec, Review of approaches for integrating loss estimation and life cycle assessment to assess impacts of seismic building damage and repair, Eng. Struct. 175 (2018) 123–137, https://doi.org/10.1016/j.engstruct.2018.08.011.
[15] V. Hasik, M. Ororbia, G.P. Warn, M.M. Bilec, Whole building life cycle environmental impacts and costs: a sensitivity study of design and service decisions, Build. Environ. 163 (2019), 106316, https://doi.org/10.1016/j.buildenv.2019.106316.
[16] Z. Shen, H. Zhou, S. Shrestha, LCC-based framework for building envelope and structure co-design considering energy efficiency and natural hazard performance, J. Build. Eng. 35 (2021), https://doi.org/10.1016/j.jobe.2020.102061.
[17] E. Asadi, Z. Shen, H. Zhou, A. Salman, Y. Li, Risk-informed multi-criteria decision framework for resilience, sustainability and energy analysis of reinforced concrete buildings, J. Build. Perform. Simul. 13 (2020) 804–823, https://doi.org/10.1080/19401493.2020.1824016.
[18] R.M.S.F. Almeida, N.M.M. Ramos, S. Manuel, Towards a methodology to include building energy simulation uncertainty in the Life Cycle Cost analysis of rehabilitation alternatives, J. Build. Eng. 2 (2015) 44–51, https://doi.org/10.1016/j.jobe.2015.04.005.
[19] S. Gavrilovic, T. Haukaas, Multi-model probabilistic analysis of the lifecycle cost of buildings, Sustain. Resilient Infrastruct. 7 (2022) 313–331, https://doi.org/10.1080/23789689.2020.1846236.
[20] R. Han, Y. Li, J. Lindt, Seismic loss estimation with consideration of aftershock hazard and post-quake decisions, ASCE-ASME J. Risk Uncertain. Eng. Syst. Part Civ. Eng. 2 (2016), 04016005, https://doi.org/10.1061/AJRUA6.0000875.
[21] S. Kc, D. Gautam, Progress in sustainable structural engineering: a review, Innov. Infrastruct. Solut. 6 (2021) 68, https://doi.org/10.1007/s41062-020-00419-3.
[22] T.L. Saaty, The Analytic Hierarchy Process: Planning, Priority Setting, Resource Allocation, McGraw-Hill International Book Company, 1980.
[23] T.-C. Wang, Y.-H. Chen, Applying consistent fuzzy preference relations to partnership selection, Omega 35 (2007) 384–388, https://doi.org/10.1016/j.omega.2005.07.007.
[24] H. Deng, Multicriteria analysis with fuzzy pairwise comparison, Int. J. Approx. Reason. 21 (1999) 215–231, https://doi.org/10.1016/S0888-613X(99)00025-0.
[25] M. Ataei, H. Shahsavany, R. Mikaeil, Monte Carlo Analytic Hierarchy Process (MAHP) approach to selection of optimum mining method, Int. J. Min. Sci. Technol. 23 (2013) 573–578, https://doi.org/10.1016/j.ijmst.2013.07.017.
[26] C.E. Shannon, A mathematical theory of communication, Bell Syst. Tech. J. 27 (1948) 379–423, https://doi.org/10.1002/j.1538-7305.1948.tb01338.x.
[27] R. Al-Aomar, A combined ahp-entropy method for deriving subjective and objective criteria weights, Int. J. Ind. Eng. Theory Appl. Pract. 17 (2010) 12–24.
[28] S. Wang, L. Ge, S. Cai, L. Wu, Hybrid interval AHP-entropy method for electricity user evaluation in smart electricity utilization, J. Mod. Power Syst. Clean Energy 6 (2018) 701–711, https://doi.org/10.1007/s40565-017-0355-3.
[29] E.S. Bakhoum, D.C. Brown, A hybrid approach using AHP–TOPSIS–entropy methods for sustainable ranking of structural materials, Int. J. Sustain. Eng. 6 (2013) 212–224, https://doi.org/10.1080/19397038.2012.719553.
[30] C.-L. Hwang, K. Yoon, Methods for multiple attribute decision making, in: C.-L. Hwang, K. Yoon (Eds.), Mult. Attrib. Decis. Mak. Methods Appl. State—Art Surv., Springer, Berlin, Heidelberg, 1981, pp. 58–191, https://doi.org/10.1007/978-3-642-48318-9_3.
[31] H. Krawinkler, E. Miranda, Performance-based earthquake engineering, Earthq. Eng. Eng. Seismol. Perform.-Based Eng. 9 (2004) 1–9.
[32] M. Ulmi, Hazus-MH 2.1 Canada, User and Technical Manual: Earthquake Module, Natural Resources Canada Ottawa, ON, Canada, 2014.
[33] ARUP, Resilience-based Earthquake Design Initiative for the Next Generation of Buildings, 2013.
[34] J. Hill, in: S.A. Levin (Ed.), Life Cycle Analysis of Biofuels, second ed.Encycl. Biodivers, Academic Press, Waltham, 2013, pp. 627–630, https://doi.org/10.1016/B978-0-12-384719-5.00365-8.
[35] S. Kubba, Chapter 8 - green design and construction economics, in: S. Kubba (Ed.), Green Constr. Proj. Manag. Cost Overs., Architectural Press, Boston, 2010, pp. 304–342, https://doi.org/10.1016/B978-1-85617-676-7.00008-7.
[36] RSMeans data: construction cost estimating software. https://www.rsmeans.com. (Accessed 15 October 2022).

[37] Abate Douglas, Michael Towers, Richard Dotz, Luca Romani, The Whitestone Facility Maintenance and Repair Cost Reference 2009-2010, Fourteenth Annual Edition, Whitestone Research, Santa Barbara, CA, 2009.
[38] Impact estimator for buildings | life cycle assessment software. https://calculatelca.com/software/impact-estimator/. (Accessed 15 October 2022)..
[39] S. Günay, K.M. Mosalam, PEER performance-based earthquake engineering methodology, revisited, J. Earthq. Eng. 17 (2013) 829–858, https://doi.org/10.1080/13632469.2013.787377.
[40] Unified hazard tool. https://earthquake.usgs.gov/hazards/interactive/. (Accessed 23 December 2022).
[41] D. Vamvatsikos, C. Allin Cornell, Incremental dynamic analysis, Earthq. Eng. Struct. Dynam. 31 (2002) 491–514, https://doi.org/10.1002/eqe.141.
[42] T.Y. Yang, J. Moehle, B. Stojadinovic, A. Der Kiureghian, Seismic performance evaluation of facilities: methodology and implementation, J. Struct. Eng. 135 (2009) 1146–1154, https://doi.org/10.1061/(ASCE)0733-9445(2009)135:10(1146).
[43] K.I. Praseeda, B.V. Venkatarama Reddy, M. Mani, Life-cycle energy assessment in buildings: framework, approaches, and case studies, in: M.A. Abraham (Ed.), Encycl. Sustain. Technol., Elsevier, Oxford, 2017, pp. 113–136, https://doi.org/10.1016/B978-0-12-409548-9.10188-5.
[44] EnergyPlus. https://energyplus.net/. (Accessed 5 October 2022).
[45] 3D design software | 3D modeling on the web | SketchUp. https://www.sketchup.com/. (Accessed 14 November 2022).
[46] OpenStudio. https://openstudio.net/. (Accessed 14 November 2022).
[47] Eppy Tutorial — eppy 0.5.62 documentation. https://eppy.readthedocs.io/en/latest/Main_Tutorial.html. (Accessed 19 December 2022).
[48] M.D. McKay, R.J. Beckman, W.J. Conover, A comparison of three methods for selecting values of input variables in the analysis of output from a computer code, Technometrics 42 (2000) 55–61, https://doi.org/10.1080/00401706.2000.10485979.
[49] R. Vasaturo, T. van Hooff, I. Kalkman, B. Blocken, P. van Wesemael, Impact of passive climate adaptation measures and building orientation on the energy demand of a detached lightweight semi-portable building, Build. Simulat. 11 (2018) 1163–1177, https://doi.org/10.1007/s12273-018-0470-8.
[50] J. Bravo Dias, G. Carrilho da Graça, P.M.M. Soares, Comparison of methodologies for generation of future weather data for building thermal energy simulation, Energy Build. 206 (2020), 109556, https://doi.org/10.1016/j.enbuild.2019.109556.
[51] D.H.W. Li, S.L. Wong, Daylighting and energy implications due to shading effects from nearby buildings, Appl. Energy 84 (2007) 1199–1209, https://doi.org/10.1016/j.apenergy.2007.04.005.
[52] Y.-W. Du, K. Gao, Ecological security evaluation of marine ranching with AHP-entropy-based TOPSIS: a case study of Yantai, China, Mar. Pol. 122 (2020), 104223, https://doi.org/10.1016/j.marpol.2020.104223.
[53] X. Chuansheng, D. Dapeng, H. Shengping, X. Xin, C. Yingjie, Safety evaluation of smart grid based on AHP-entropy method, Syst. Eng. Procedia. 4 (2012) 203–209, https://doi.org/10.1016/j.sepro.2011.11.067.
[54] Y. Zhu, D. Tian, F. Yan, Effectiveness of entropy weight method in decision-making, Math. Probl Eng. 2020 (2020), e3564835, https://doi.org/10.1155/2020/3564835.
[55] H. Díaz, A.P. Teixeira, C. Guedes Soares, Application of Monte Carlo and Fuzzy Analytic Hierarchy Processes for ranking floating wind farm locations, Ocean Eng. 245 (2022), 110453, https://doi.org/10.1016/j.oceaneng.2021.110453.
[56] FEMA, FEMA 355 State of the Art Report on Systems Performance of Steel Moment Frames Subject to Earthquake Ground Shaking, Rep No FEMA-355C, 2000.
[57] R. Sabelli, Research on Improving the Design and Analysis of Earthquake-Resistant Steel-Braced Frames, EERI Oakland, CA, USA, 2001.
[58] Y. Ohtori, R.E. Christenson, B.F. Spencer, S.J. Dyke, Benchmark control problems for seismically excited nonlinear buildings, J. Eng. Mech. 130 (2004) 366–385, https://doi.org/10.1061/(ASCE)0733-9399(2004)130:4(366).
[59] T. Lou, W. Wang, Life cycle environmental evaluation of steel frames for performance-based seismic assessment, in: Life-Cycle Civ. Eng. Innov. Theory Pract., CRC Press, 2020.
[60] Standard 90.1. https://www.ashrae.org/technical-resources/bookstore/standard-90-1. (Accessed 14 November 2022).
[61] F. McKenna, OpenSees: a framework for earthquake engineering simulation, Comput. Sci. Eng. 13 (2011) 58–66, https://doi.org/10.1109/MCSE.2011.66.
[62] L.F. Ibarra, Global Collapse of Frame Structures under Seismic Excitations, Stanford University, 2004.
[63] D.G. Lignos, H. Krawinkler, Deterioration modeling of steel components in support of collapse prediction of steel moment frames under earthquake loading, J. Struct. Eng.-Rest. 137 (2011) 1291.
[64] FEMA, Quantification of Building Seismic Performance Factors, 2009. Washington D.C.
[65] D. Zhuang, X. Zhang, Y. Lu, C. Wang, X. Jin, X. Zhou, X. Shi, A performance data integrated BIM framework for building life-cycle energy efficiency and environmental optimization design, Autom. ConStruct. 127 (2021), 103712, https://doi.org/10.1016/j.autcon.2021.103712.
[66] T. Tan, G. Mills, E. Papadonikolaki, Z. Liu, Combining multi-criteria decision making (MCDM) methods with building information modelling (BIM): a review, Autom. ConStruct. 121 (2021), 103451, https://doi.org/10.1016/j.autcon.2020.103451.
[67] R. Santos, A.A. Costa, J.D. Silvestre, L. Pyl, Integration of LCA and LCC analysis within a BIM-based environment, Autom. ConStruct. 103 (2019) 127–149, https://doi.org/10.1016/j.autcon.2019.02.011.